

INTEGRATED ANALYSIS AND APPLICATION OF RESERVOIR MODELS TO  
EARLY PERMIAN DETRITAL CARBONATE DEPOSITS, MIDLAND BASIN,  
TEXAS

A Thesis

by

TRAVIS WAYNE JOHNSTON

Submitted to the Office of Graduate Studies of  
Texas A&M University  
in partial fulfillment of the requirements for the degree of

MASTER OF SCIENCE

Approved by:

Chair of Committee,	Michael C. Pope
Committee Members,	Ernest A. Mancini
	Yuefeng Sun
	David S. Schechter
Head of Department,	Rick E. Giardino

December 2012

Major Subject: Geology

Copyright 2012 Travis Wayne Johnston

## ABSTRACT

A 3-D seismic volume, wireline logs and core data were integrated to determine the spatial distribution of porous reservoirs within the Wolfcampian-Leonardian detrital carbonate slope and basin strata in Glasscock County, Texas. A 3-D seismic amplitude volume was used to construct a seismic facies analysis of the detrital carbonate section, and generated attribute volumes helped identify detrital carbonate depositional trends, as well as establish a potential correlation between thick detrital carbonate intervals and associated amplitude response.

Eight lithofacies were identified in core and were subsequently classified into three main facies: *debris flow*, *grain flow/turbidite*, and *basinal shale*. A facies type log was then created, which was used to supervise the creation of facies logs within other wells to ultimately use in the creation of a 3-D facies model. Cross sections through the study area show an increase in bathymetric relief beginning in Wolfcampian time and continuing through the Leonardian. Detrital carbonate deposition increases dramatically during the Leonardian, consisting of large gravity flows deposited basinward in a northwest-southeast linear trend, rapidly thinning basinward. Individual flows are discontinuous and bounded by *basinal shale* facies.

Four seismic facies were identified within the interval of interest using a structurally smoothed attribute volume, while an RMS amplitude attribute volume provided a correlation between high RMS amplitude values and detrital carbonate

thickness. A high RMS amplitude value corresponding to the *debris flow* facies was extracted from the RMS attribute volume in the form of a seismic geobody.

Two facies models and one porosity model were generated by using upscaled values from the gamma ray, total porosity, and lithofacies logs, which were applied over areas with the densest well control. Although the facies model populated from upscaled GR values was useful in stratigraphic interpretation, it is determined that the models should be applied over areas with denser well spacing in order to provide a more accurate and geologically viable subsurface model.

## DEDICATION

To my family and friends, for everything.

## ACKNOWLEDGEMENTS

I would like to thank my committee chair, Dr. Pope, and my committee members, Dr. Mancini, Dr. Sun, and Dr. Schechter, for their guidance and support throughout the course of this research.

I would also like to give thanks to my friends, colleagues and the department faculty and staff for making my time at Texas A&M University a great experience. I also want to extend my gratitude to John Polasek and Apache Corporation, who provided the data to complete this thesis, and to James Donnelley and Andrew Faigle at the Texas Bureau of Economic Geology Core Research Center.

Finally, thanks to Mom and Dad for their bulk financial support and never ending love and encouragement through the years.

## NOMENCLATURE

AI	Acoustic Impedance
bbbl	Barrels of Oil
cm	centimeter
DT	Acoustic Travel Time (measured in microseconds/foot)
ft	Feet (length)
$f$	Frequency (measured in Hertz)
GR	Gamma Ray (measured in API units)
GRFS	Gaussian Random Function Simulation
GRlog	Gamma Ray measured from log (measured in API units)
GRmax	Gamma Ray of 100% shale interval (measured in API units)
GRmin	Gamma Ray of shale free interval (measured in API units)
HST	Highstand Systems Tract
$\lambda$	Wavelength
Hz	Hertz
IGR	Gamma Ray Index (unitless)
LST	Lowstand Systems Tract
m	Meter (length)
Ma	Measurement of Time ( $1 \times 10^6$ years)
NPHI	Neutron Porosity (unitless)
NPHIshale	Porosity value of shale formation (unitless)

PE	Photoelectric factor (measured in barns/electron)
PHIC	Corrected Porosity (unitless)
PHIT	Total Porosity (unitless)
RHOB	Bulk Density (measured in grams/cubic centimeter)
RMS	Root Mean Squared
SGS	Sequential Gaussian Simulation
SIS	Sequential Indicator Simulation
SP	Spontaneous Potential (measured in millivolts)
SwT	Water Saturation (measured in percent)
t	One-Way-Time (measured in seconds)
TEM	Train Estimation Modeling
TWT	Two Way Time (measured in seconds)
Vshale	Volume of shale (measured in percent)
$\Delta z$	Interval Thickness (measured in feet)

## TABLE OF CONTENTS

	Page
ABSTRACT .....	ii
DEDICATION .....	iv
ACKNOWLEDGEMENTS .....	v
NOMENCLATURE .....	vi
TABLE OF CONTENTS .....	viii
CHAPTER I INTRODUCTION .....	1
Introduction .....	1
Geologic Setting .....	3
CHAPTER II METHODS .....	7
Core Description .....	7
Well Log Correlation and Formation Evaluation .....	7
Seismic Analysis .....	8
Three Dimensional Reservoir Modeling .....	9
CHAPTER III ANALYSIS OF WOLFCAMPIAN-LEONARDIAN DETRITAL CARBONATES .....	10
Core Description .....	10
Well Log Correlation and Formation Evaluation .....	12
Seismic Analysis .....	21
Three Dimensional Reservoir Modeling .....	27
CHAPTER IV DISCUSSION .....	31
Proposed Depositional Models .....	31
Timing of Deposition/Mechanisms for Transport .....	32
Seismic Resolution of Detrital Carbonate Reservoirs .....	34
Viability of Utilizing 3-D Reservoir Modeling .....	36



	Page
CHAPTER V CONCLUSIONS .....	37
Summary .....	37
REFERENCES .....	39
APPENDIX A .....	42
APPENDIX B .....	48
APPENDIX C .....	51
APPENDIX D .....	75

# CHAPTER I

## INTRODUCTION

### Introduction

The Permian Basin of west Texas and southeast New Mexico has produced hydrocarbons for over 80 years, and remains the third largest petroleum-producing province of the United States, trailing only offshore Gulf of Mexico and Alaska (Dutton et al., 2005). Considered by most as a “mature” petroleum basin in regards to its cumulative production, the Permian Basin continues to play a vital role in supplying the nation’s ever-increasing demand for fossil fuels. An estimated remaining reserves potential from the productive resource base of conventional reservoirs in Pennsylvanian-Permian strata is in excess of 3 billion bbl, not including reserve estimates from the recent unconventional reservoir development (Dutton et al., 2005). However, future development from these prolific conventional reservoirs is dependent on our ability to effectively understand and characterize the dynamics of the subsurface system using available data, and to develop new play concepts and methods of resource recovery for use in future drilling programs.

The introduction of sequence stratigraphic concepts developed in the 1970’s by the Exxon research group (Vail et al., 1977) created a paradigm shift in the way hydrocarbon exploration and development were conducted. Sequence stratigraphy applied to both well log and seismic interpretation has expanded our understanding of the overall stratigraphic evolution of sedimentary basins through time, as well as

provided a method for predicting the location of hydrocarbon reservoirs. During the 1970's, the first ever 3-D seismic surveys were collected for hydrocarbon exploration (Brown, 2004). 3-D seismic data significantly enhanced structural and stratigraphic interpretations of the subsurface, resulting in increased well success rates. For example, the implementation of a 14 square mile 3-D seismic survey by Trend Exploration in Glasscock County, Texas increased well success rate from 14% to 59% from 42 drilled wells, increasing reserves by 10.5 million barrels of oil (Montgomery, 1996).

Detrital carbonate sediments derived from adjacent shallow water carbonate shelf margins have been of scientific and economic interest for many years (Cook and Enos, 1977). These sediments not only serve as prolific reservoirs for hydrocarbon accumulation, but are studied to understand sea level fluctuations and the processes involved in the shedding of carbonate material into basinal environments.

The Permian Basin of Texas and southeastern New Mexico is a world class location to study detrital carbonate sediments. The Lower Permian section of the Permian Basin consists of Wolfcampian to Lower Guadalupian debris flows, gravity flows, and other associated mass wasting events derived from shallow water shelf margin facies. Outcrop studies characterize the Permian detrital carbonate section exposed in the mountains of West Texas adjacent to the Delaware Basin (Playton and Kerans, 2002). However, there are no Permian outcrops adjacent to the Midland Basin, and studies of these rocks rely on the abundance of subsurface data acquired from decades of hydrocarbon exploration. Previous studies of the Early Permian section in Glasscock County, Texas include Leary and Feeley (1991), Montgomery (1996), Stouder

(1998), and Flamm (2008). Detrital carbonate reservoirs in the Permian Basin have been exploration targets for the petroleum industry since the 1960's (Leary and Feeley, 1991). These stratigraphically controlled reservoirs are well known along the Eastern Shelf, Central Basin Platform, and southeastern Delaware Basin (Montgomery, 1996). Due to its position straddling the Eastern Shelf and the eastern Midland Basin, Glasscock County contains significant production from Lower Permian detrital carbonate reservoirs. Productive wells in Powell Ranch Field can produce 400-1200 bbl of high gravity oil a day, with reserves ranging from 0.2 to 1.3 million barrels of oil (Montgomery, 1996). Although the utilization of three dimensional seismic data has undoubtedly increased the success rate of drilled wells, there remains a need to better understand and characterize abrupt facies changes and overall reservoir distribution of these detrital systems (Montgomery, 1996). This study presents a three dimensional facies model of Lower Permian detrital carbonate sediments in Glasscock County, Texas, created by integrating facies descriptions obtained from cores with well log values from the gamma ray and neutron logs. Additionally, a 3-D seismic survey is used to analyze reflection patterns within the detrital carbonate section in order to better understand detrital carbonate deposition and spatial patterns.

### Geologic Setting

The Permian Basin of southwestern United States is a Late Paleozoic sedimentary basin that underlies the regions of west Texas and southeastern New Mexico, covering approximately 115,000 square miles (Mazuingue-Desailly, 2004). The Permian Basin is the westernmost of the Paleozoic foreland basins formed as a

result of continental collision of Laurentia with the northwestern portion of Gondwana during the Marathon-Ouachita orogenic event. It is structurally subdivided into several sub-basins (Figure 1) by fault-bounded intraforeland uplifts of the Central Basin Platform, Diablo Platform, and Ozona Arch (Yang and Dorobek, 1995). Permian Basin formation began over a preceding sedimentary basin, the Tobosa Basin, which occupied the same area. This shallow, semicircular depression probably formed during the Late Precambrian-Early Cambrian, and was actively subsiding from the Cambrian to Mississippian (Yang and Dorobek, 1995). The Tobosa Basin was subsequently fragmented into the sub-basins bounded by several prominent intraforeland uplifts during Late Mississippian-Pennsylvanian continental collision. The Diablo Platform separates the Marfa Basin and Delaware Basin, the Central Basin Platform divides the Delaware and Midland Basins, and the Ozona Arch divides the southern Midland Basin from the Val Verde Basin. In addition to loading caused by the Marathon-Ouachita thrust sheets, the intraforeland uplifts created additional topographic loads that resulted in differential basin geometries (Yang and Dorobek, 1995). Collisional tectonics occurred through the Wolfcampian, and by the Middle to Late Permian, the Permian Basin entered a period of tectonic quiescence characterized by slowed subsidence and sediment infilling of the sub-basins. Late Mesozoic-Early Cenozoic Laramide orogenic forces uplifted and tilted the western margin of the Permian basin toward the east (Horak, 1985).

Stratigraphic evolution of the Permian Basin reflects a complex, mixed carbonate-siliciclastic system transitioning from an early to middle Paleozoic ramp a late

Paleozoic distally steepened ramp and rimmed shelf environment. Facies distribution and thickness variations among strata vary widely, coincident with the subsequent tectonic evolution of the Permian Basin and its related intraforeland uplifts, most notably the Central Basin Platform. This study focuses primarily on the Lower Permian section of detrital limestones and interbedded basinal facies of the Wolfcampian and Lower Leonardian (Figure 2). The Desmoinesian Strawn Limestone is a shallow water carbonate of fairly constant thickness across much of the Permian Basin that supports the interpretation of carbonate ramp deposition during the Early and Middle Paleozoic (Yang and Dorobek, 1995). Large thickness variation in the Upper Pennsylvanian and Wolfcampian strata overlying the Strawn Limestone reflect deposition during a time of increased differential subsidence in the basin, most likely due to increased tectonic load generated by the uplift of the Central Basin Platform. The transition from a ramp to a distally steepened ramp and rimmed shelf margin begins in the upper Pennsylvanian-Wolfcampian with shallow water carbonate deposition occurring along the basin margins and deepwater siliciclastics and lime mud deposition occurring in deeper areas of the basin. Reef building organisms such as phylloid algae, sponges, and *Tubiphytes* contributed to the development of rimmed shelves during a time in which global icehouse conditions dominated. As reef growth increased, shallow water carbonate material was transported and deposited basinward, forming a detrital apron along the toe-of-slope environment (Cook and Mullins, 1983). These allochthonous carbonate sediments typically occur as thick accumulations of shallow water clasts and skeletal debris interbedded with basinal siliciclastics. Rapid progradation of these rimmed shelf

margins during the Permian resulted in the infilling of all available accommodation space of the Permian Basin by the end of the Guadalupian (Mazzullo, 1997).

Stratigraphic assignment of Wolfcampian age strata in the Permian Basin is controversial. Wolfcampian rocks of North America are Asselian and Sakmarian (Flamm, 2008). Particularly in the petroleum industry, the productive “Wolfcamp” section consists of shelf-derived detrital carbonate debris flows and grain flows interbedded with basinal shale and lime mudstone (Montgomery, 1996). Fusulinid biostratigraphy suggests that the detrital section between the “Wolfcamp Shale” and the overlying Dean Sandstone is Leonardian in age, contradicting the previous interpretation of Wolfcampian age (Mazzullo, 1997). Therefore, the top of the “Wolfcamp Shale” is used to define the boundary between uppermost Wolfcampian and lowermost Leonardian for this study.

Wolfcampian and Leonardian strata in the Midland Basin form distinct progradational packages, as successive carbonate shelf margins prograded basinward during the Permian. Subjacent to these steep-rimmed margins are thick sections of periplatform carbonate. This study focuses on the Wolfcampian-Leonardian detrital section of the eastern Midland Basin in Glasscock County, Texas (Figure 3). This study establishes a three dimensional model that identifies detrital carbonate facies and their spatial occurrences by integrating core description, well log and seismic data. Relationships between well logs are used to identify depositional facies, and seismic amplitude signatures of the Wolfcampian-Leonardian section are characterized; several seismic attributes were created and used to identify detrital carbonate occurrences.

## CHAPTER II

### METHODS

#### Core Description

Four conventional slabbled cores from within or close to the study area in Glasscock County (Figure 4) were described for this study in order to characterize the Wolfcampian-Leonardian detrital carbonate deposits. Cored sections range from the Upper Pennsylvanian through the Lower Leonardian carbonate detrital interval overlying the Wolfcamp Shale. Lithofacies were described using the Dunham (1962) classification with modification by Embry and Klovan (1971). Grain types, grain size, grain shapes, sorting, and the occurrence and abundance of sedimentary structures, graded bedding, and fractures also were described. The cores were described at the Bureau of Economic Geology core facility in Midland, Texas. Data from an additional cored well in the field, courtesy of Apache Corporation, was used to supplement the interpretation.

#### Well Log Correlation and Formation Evaluation

Well logs were used to correlate formation tops and define depositional facies in the study area, and petrophysical calculations from well log data were used to evaluate porosity values in the Wolfcampian-Leonardian section. Sonic and density logs were used to establish a time-depth relationship between well log interpretations in depth and the time horizons picked in the 3-D seismic volume.



For this portion of the project, 157 wells with associated digital log data that penetrate the top of the Wolfcampian section (Figure 5) were loaded into Petrel 2011<sup>©</sup>. These wells were used for the interpretation of formation tops and the construction of strike and dip oriented cross sections across the study area. A number of these wells are located to the north of the seismic survey, and are interpreted in order illustrate the change in relief associated with the transition from the basin to slope setting of the Wolfcampian shelf margin in Glasscock County. An additional 296 wells (Figure 5) containing total porosity (PHIT) values were later loaded into the project. These wells were used in the facies and petrophysical property modeling process.

### Seismic Analysis

A 3-D seismic survey was donated by Apache Corporation and loaded into Petrel 2011<sup>©</sup> to interpret seismic facies in the study area. The 3-D survey covers approximately 146 square miles (93,367 acres) in southern Glasscock County. The 3-D acquisition grid is made up of 611 east-west inlines and 826 north-south crosslines, with a receiver spacing and bin size of 110 feet and 55 feet, respectively. Line and trace length is variable due to the non-rectangular shape of the survey, with lines ranging from 5-17 miles long and traces 6-10.5 miles long. Sampling rate of the seismic is 2 milliseconds, with a recording interval of 3 seconds. Based on an extracted wavelet from the Garden City #1 well (Figure 6), the seismic data is normal polarity and 51 degrees out of phase from zero phase. Dominant frequency was determined to be approximately 32 Hz, with a bandwidth of 10-60 Hz.

Vertical slices were used to interpret four horizons within the area. Vertical sections were also used in conjunction with time slices to complete a basic seismic facies analysis of the Wolfcampian-Leonardian detrital carbonate interval, describing reflection patterns and geometry. Additionally, a number of amplitude related attribute volumes were created in an attempt to identify individual mass wasting events from seismic and to characterize their overall geometry.

### Three Dimensional Reservoir Modeling

By integrating physical rock descriptions, well log and petrophysical analysis, and seismic reflection data, 3-D models of the Early Permian lower slope and basinal depositional environment were generated. Through the upscaling process, values were assigned to individual cells in a 3-D grid that were penetrated by the wellbores (Schlumberger, 2010). These values are assigned based on the average value of the property being modeled over an interval equivalent to the thickness of the 3-D grid cell. This is done over the entire interval of interest, and all cells intersected by a wellbore were assigned a value. The resolution of a 3-D model is dependent on the cell dimension, which determines the number of cells contained within the 3-D grid. Two different algorithms were used to populate the upscaled properties into the 3-D grids. The algorithms were chosen based on the overall size of the survey area and the amount of data available across the survey area. The Sequential Indicator Simulation (SIS) algorithm was used for populating the discrete data (facies logs), while the Gaussian Random Function Simulation (GRFS) algorithm was used to populate the continuous data (raw log data).

## CHAPTER III

### ANALYSIS OF WOLCAMP-LEONARDIAN DETRITAL CARBONATES

#### Core Description

A total of 541ft. (165 m) of Wolfcamp-Leonard section was described from four conventional slabbed cores in Glasscock County. Three cores from nearby Powell Ranch Field were described in addition to one core within the study area. Additional in-house core data from Apache Corporation was used to supplement the interpretations. Refer to appendix A for illustrations and photos of all core described for this study.

Nine facies were identified from core descriptions. These facies were then grouped into the three depositional settings: 1) *basinal deep water*, 2) *detrital apron debris flow*, and 3) *detrital apron grain flow/turbidite*. These classifications were based on similarities between described facies and interpreted depositional environment. A brief description of each facies (1-8) is summarized in Table 1.

Facies 2, 3, and 6 are interpreted as a *basinal deep water* facies that occur in the deeper, low energy environments of the basin. Fine-grained siliciclastic and carbonate deposition occurs from settling out of the water column and occasional distal turbidite events. These facies are typically finely laminated and have few signs of higher energy deposition other than the occasional interbedded thin, often graded beds of calcisiltstone-fine sandstone turbidity currents. Fossils typically are sparse, and consist primarily of brachiopod fragments, fusulinids, and small crinoid fragments. Occasional 1-3 cm thick skeletal wackestone/packstone beds, pyrite and phosphate nodules also occur in this

facies. The dark gray to black color and the presence of pyrite and phosphate infers a dysoxic to anoxic depositional setting where organic matter was preserved. The prolific Early Permian detrital reservoirs of the Permian Basin are sourced directly by these organic-rich basinal shales (Montgomery 1996; Mazzullo, 1997).

Facies 1, 5, and 7 are interpreted as a *detrital apron debris flow* facies in which large amounts of shallow water material derived from the shelf edge and upper slope are transported downslope and deposited along the toe-of-slope and further into the basin during mass wasting episodes (Cook and Mullins, 1983). The clasts originated in shallow water as indicated by their fossils. These clasts often are several centimeters in diameter and contain numerous reef builders and other shallow water organisms, including sponges, phylloid algae, bryozoans, large crinoids, fusulinids, brachiopods, ostracodes, and gastropods. Clasts generally are poorly sorted and are randomly oriented. Occasional post-depositional transport is indicated by overturned geopetal structures. Clast-supported conglomerates were the most common type of debris flow observed, with only a few matrix supported conglomerates occurring. Two different matrix types were observed in the *detrital apron debris flow* facies; the first is a pelletal-skeletal packstone/grainstone of facies 4 and 8, the other was a dark shale/mudstone matrix of facies 1, 5, and 7. These facies were observed in three of the described cores, and the Powell "C" 1 core was composed entirely of debris flow facies (Figure 7). The *detrital apron debris flow* facies is interpreted as originating along the shelf edge and upper slope and being subsequently deposited onto the lower to middle part of the slope via sediment gravity transport processes.

Facies 4 and 8 are interpreted as a *detrital apron grain flow/turbidite* facies formed during mass wasting events as concentrated grain flows of shallow water derived sand sized carbonate grains that are deposited along the toe of slope and out in the basin. Grain flows and distal turbidites were observed in the E. L. Powell #1 (Appendix A) and J. W. Cox #1 (Figure 8) cores. Fossil types within these facies are primarily of shallow water origin, including coarse grained pellets and crinoid fragments, brachiopods, fusulinids, peloids, and ostracods. Occasional reef clasts include sponges, phylloid algae, and bryozoans. This facies is massively bedded, lacking any visible sedimentary structures. This facies occurs as a relatively thick, homogenous section as opposed to thinner intervals interbedded with basinal shales and mudstones. This suggests that this facies occurs as channelized grain flows that occur more continuously as opposed to individual events of isolated grain flows. These carbonate sands also are most likely confined to channels as they are transported and may deposit in lobate fan geometries in the basin (Mazzullo, 1997).

#### Well Log Correlation and Formation Evaluation

Lithostratigraphic correlation techniques were used to interpret 152 well logs in the project area in order to identify the tops of the Upper Cline Shale, the Wolfcamp Shale, the Dean Sand, and the Wichita/Albany. The top of the Spraberry Sand also was interpreted in a number of wells for stratigraphic constraint, but was not a focus of this project. Dip sections through the study area (Figures 9-10) show the 1) gross structure of the study area relative to Upper Pennsylvanian-Lower Leonardian units, 2) increase in bathymetric relief from the basin floor to the middle slope and shallow shelf area of the

Wolfcampian shelf margin, and 3) relative decrease in Leonardian detrital carbonate sediments moving basinward. Correlation techniques used on section B-B' (Figure 10) illustrate the spatial distribution and continuity of detrital carbonates deposited on the slope and basin in Glasscock County.

Facies interpreted from well log signatures are made based on the interpretation of facies from core descriptions. Additionally, a *siltstone* facies is used for correlation of the Dean Sandstone, which was deposited during sea level lowstand within the Lower Leonardian detrital section (Mazzullo, 1997), but was not present in core. Depositional and lithological characteristics of the Wolfcamp and Leonardian sections are noticeably different, and reflect the different depositional environments of their respective times.

For this study, the Wolfcamp section is interpreted as occurring between the underlying Upper Cline Shale and the overlying Lower Leonardian detrital section. The Wolfcamp section consists of high gamma ray (GR) basinal shales and thin interbedded grain flows/turbidites and debris flows with low to medium GR values. Blocky, fining upward, and coarsening upward GR profiles all occur in the detrital facies of the Wolfcamp section across the area. Average thickness of the grain flow/turbidite interbeds is 2-5 ft (0.5-2 m), which is relatively constant across the area. The thickest detrital carbonate sections are discontinuous across the study area, and range in thickness from 20-80 ft (6-24 m). Porosity values in the debris flow and grain flow/turbidite facies range from 2-11% as seen on the NPHI log.

The Wolfcampian and Leonardian sections are very different from each other. Within the Lower Leonardian itself, lithological heterogeneity increases

westward, reflecting a transition between the toe-of-slope and the basin floor. For this study, the Lower Leonardian section is interpreted as the detrital section bounded by the underlying Wolfcampian section and the overlying Spraberry Sands. The Lower Leonardian section includes the Dean Sandstone, which is the basinal equivalent of the Tubb or middle Clearfork sand on the Central Basin Platform and Northern Platform (Mazzullo, 1997). In the northeast portion of the study area, Lower Leonardian strata consists primarily of low GR detrital carbonate debris flow and grain flow facies with interbedded with thin bedded, high GR basinal shales. A blocky GR profile is most prevalent, and the observation of sharp contacts between the detrital carbonate and basinal shale suggests that detrital carbonate deposition occurred episodically. Debris flow and grain flow facies are much thicker than in the underlying Wolfcampian section, ranging from 2-200 ft (0.5-61 m). In some detrital sections, the GR values are somewhat high, and are interpreted as a matrix-supported debris flow facies. Porosity values are somewhat lower than the Wolfcamp detritals, ranging from 1-6%. However, a large positive deflection in the SP, separation of the shallow and deep resistivity curves and observed “gas effect” in the porosity logs indicate permeability and presence of hydrocarbons. Lithology changes considerably moving west into the basin. Here, the detrital carbonates of the Leonardian section are thinner and interfinger with high GR basinal shales. Thickness of the individual detrital sections typically range from 2-20 ft (0.5-6 m), with the thickest being 100 ft (30 m). These thicker debris flow/grain flow sections are not laterally extensive. An SP deflection is not seen in most beds due to

their thickness, but “gas effect” is observed in most detrital sections. Porosity values of these facies range from 2-4% on the neutron logs.

A periplatform carbonate facies model proposed by Mazzullo (1997) suggests that a diagenetic transition from limestone to mainly dolomite occurs updip in the detrital apron. Since photoelectric factor (PE) values were not always helpful in determining lithology, a crossplot of bulk density (RHOB) and neutron porosity (NPHI) created by Halliburton (Heysse, 1983) was used in an attempt to analyze detrital carbonate lithology in four wells along depositional dip in order to test the limestone-to-dolomite diagenetic trend and to compare the values with observed photoelectric PE values from logs (Figure 11). The results of the crossplots indicate mostly limestone intervals, but with some dolomite intervals through the Wolfcampian-Leonardian detrital carbonate section. Those sections identified as dolomite from the crossplot may indicate debris flows containing non-porous slide blocks or reefal clasts that were partially to completely dolomitized prior to transport or intervals that were dolomitized postdepositionally (Mazzullo, 1997). A more comprehensive discussion of the complex diagenetic sequence of the Lower Permian detrital carbonates in the Midland Basin is presented in Mazzullo (1994c), Mazzullo and Harris (1991), and Mazzullo and Reid (1987). Due to the presence of gas in many of the detrital intervals and its effects on NPHI, only a limited number of sample intervals were crossplotted. Based on these results, the limestone-to-dolomite transition proposed by Mazzullo (1997) cannot be confidently identified using a RHOB vs. NPHI crossplot in the study area.



The Upper Wolfcamp boundary was picked on a prominent gamma ray log marker known as the “Wolfcamp Shale”, and is interpreted to approximate shelf-to-basin relief at the beginning of the Leonardian (Mazzullo, 1997). Topographic relief for this study was calculated based on formation tops correlated in well logs, and was estimated at approximately 2000 ft (610 m) over a distance of 6.5 miles (10.5 km). This measurement coincides with previous estimations of paleobathymetric relief of the Leonardian shelf margin (Montgomery, 1996). Based on calculations from Upper Wolfcamp surface, the gradient for the toe-of-slope and basin is approximately 1-1.5° dip. Moving eastward onto the slope, the gradient is calculated to rise to approximately 4-5° dip. In order to better illustrate thickness variation through the Wolfcamp-Leonard section, a gross isochore map was generated based on correlated well tops of the Upper Cline and Base Spraberry (Figure 12). The Wolfcamp-Leonardian thickness increases approximately 1500 ft (457 m) eastward across the study area. Only gradual thinning of the Leonardian section occurs to the west towards the middle of the basin, but the relative concentration of detrital-to-shale material decreases significantly.

Based on these interpretations of the Wolfcampian-Leonardian section, it is most appropriate to apply the *detrital apron* depositional models of Mullins and Cook (1986) and Mazzullo (1997). The *detrital apron* model argues for a line sourced apron of shelf-derived detrital carbonates forming a sediment wedge along the lower slope and toe-of-slope environments, thinning upwards onto the middle and upper slope as well as basinward.

A 3-D facies model of the Wolfcampian-Lower Leonardian detrital carbonates in the study area was generated based on facies descriptions from core and well logs. To create a facies model for the study, a facies type log was created in the Kohl #1 well based on our lithostratigraphic interpretation as well as previous work (Montgomery, 1996). Facies interpretation was completed from the Upper Cline Shale section to the base of the Spraberry Sand using three facies: 1) *basinal shale*, 2) *detrital carbonate*, and 3) *sand/siltstone*. After recreating the facies log of Montgomery (1996), the Train Estimation Modeling (TEM) process in Petrel 2011<sup>©</sup> was used to generate a discrete log that created 3 facies classes based on the correlations of gamma ray (GR) and sonic (DT) logs. These logs were used for the classification process for several reasons: 1) GR and DT measurements approximated lithology, 2) The dataset contained a large number of wells with GR and DT logs, and 3) GR and DT are less affected by borehole rugosity and reservoir fluids than other types of logs. Although utilizing a photoelectric log (PE) for lithology identification likely would have been useful, there were not enough PE logs available to warrant using them in this process.

After TEM was applied to the Kohl #1 type log, the generated classifications were compared to the manual interpretation of Montgomery (1996). In order to avoid discrepancies in the TEM process, the manual interpretation and classification logs were compared and subsequently edited to best fit the classifications based on GR and DT logs. Facies from the manual interpretation were then assigned to the classification log (Figure 13). The edited Kohl #1 facies type log was then used to create a discrete facies log in all wells within the study area containing GR and DT logs.

To better estimate effective porosity of the formation, the “shale effect” observed in the neutron porosity (NPHI) logs was removed. The “shale effect” occurs in porosity logs as a result of the neutron log measuring hydrogen concentration within the pore space as well as hydrogen concentration within the crystal lattice of clay particles in shale formations, which leads to an overestimation of porosity (Asquith and Krygowski, 2004). For this study, the purpose of correcting the porosity logs was to establish a more accurate estimation of effective porosity within the *detrital apron debris* flow facies that sometimes contains a muddy matrix. A linear calculation of the volume of shale ( $V_{\text{shale}}$ ) within a formation can be determined if the GR response of a formation assumed to contain 0% shale ( $GR_{\text{min}}$ ) and 100% shale ( $GR_{\text{max}}$ ) are measured (Asquith and Krygowski, 2004). Using the following equation, a gamma ray index ( $I_{\text{GR}}$ ) can be calculated over an entire interval using the gamma ray log ( $GR_{\text{log}}$ ).

$$V_{\text{shale}} = I_{\text{GR}} = (GR_{\text{log}} - GR_{\text{min}}) / (GR_{\text{max}} - GR_{\text{min}}) \quad 3.1$$

Based on a histogram plot of GR values, a  $GR_{\text{min}}$  of 25 and a  $GR_{\text{max}}$  of 120 was chosen. Since the interval of interest consists of older, consolidated rocks and most likely does not follow a linear trend, a nonlinear estimation was needed in order to correct the  $V_{\text{shale}}$  estimation. The Larionov correction for older rocks was considered most appropriate, and is typically used for older, more consolidated rocks (Larionov, 1969).

$$V_{\text{shale}} = 0.33 (2^{2 \times I_{\text{GR}}} - 1.0) \quad 3.2$$

Finally, a corrected porosity (PHIC) was calculated from the neutron porosity log (NPHI) and the porosity value for a shale formation using Dewan's equation (Dewan, 1983). For sensitivity analysis, three different PHIC values were calculated using  $\text{NPHI}_{\text{shale}}$  readings of 0.25, 0.30, and 0.40.

$$\text{PHIC} = \text{NPHI} - (V_{\text{shale}} \times \text{NPHI}_{\text{shale}}) \quad 3.3$$

The corrected porosity (PHIC) logs indicate that this can be an effective “acid test” method for estimating effective porosity within the study area. Results from the porosity correction are illustrated in track 3 of the log in Figure 14. Of the three calculations, the PHIC value calculated with an  $\text{NPHI}_{\text{shale}}$  value of 0.30 was determined to be the most accurate. PHIC values within the low GR detrital intervals are similar to values measured by the NPHI log. This is expected due to the fact that the low GR detrital intervals are interpreted to have minimal clay volume within the rock matrix. PHIC values tend to be within 0.01 of NPHI values in these intervals. PHIC values within the higher GR intervals are observed to be lower than the NPHI measurements. This suggests that Dewan's equation effectively removed the “shale effect” from the measurement, allowing for a more accurate estimation of effective porosity. This is primarily evident in the highest GR intervals interpreted as basinal shale facies. The calculated PHIC values give a more accurate representation of porosity, but it is

unreasonable to think these values reflect true formation porosity without core porosity data.

Although this method of porosity estimation was quick, simple and showed positive results, several observations from the logs indicate that this most likely is not the most effective method for porosity estimation, particularly when performing a detailed formation evaluation within the area. Some low GR detrital intervals show anomalously low PHIC values due to the presence of light hydrocarbons within the pore space. This “gas effect” occurs when the NPHI reads a low value due to the presence of gas in the pore space as opposed to water (Asquith and Krygowski, 2004). As a result, PHIC values tend to be underestimated, presenting a critical problem with the proposed method of porosity estimation because it is important that porosity values are accurate within a hydrocarbon bearing interval. Additionally, PHIC values within the high GR intervals tend to be negative. This is related to the fact that the shale baseline ( $GR_{max}$ ) used to estimate  $V_{shale}$  was determined by qualitatively picking an average GR value from all wells within the study area to represent 100% shale, which most likely leads to well-to-well variation in porosity estimation for the same interval.

Interpretations made from the formation evaluation suggests that even though this method could be a useful quick look method, a more sophisticated approach should be considered in order to accurately determine effective porosity within high GR intervals and within intervals that show “gas effect”. An alternate method would be to perform the same method of porosity estimation on a well-by-well basis, effectively providing more accurate estimates of  $GR_{min}$  and  $GR_{max}$  for local  $V_{shale}$  estimates. This

type of approach may be useful, especially when considering the complex lithology of the study area. A more robust method of determining porosity in the study area would be to solve for  $V_{\text{shale}}$  using a computed GR value that has removed the uranium contribution to the GR tool and reads only the potassium and thorium contributions. Uranium salts can be highly concentrated within a formation, particularly in strata with high organic content (shales). This can lead to GR values that do not accurately reflect clay content of the formation (Glover, 2000).

Using a standardized set of porosity values within the study area was important for the generation of a 3-D porosity model. Due to the uncertainty related to the previous discussed attempt to correct porosity values, it was determined that using a subset of wells that had undergone a more robust method of porosity calculation would be more useful for the project. Therefore, a suite of 161 logs containing calculated total porosity values was provided by Apache Corporation. This set of PHIT values were calculated using a  $V_{\text{shale}}$  estimation from spectral gamma ray. Total porosity is the percent of total volume of a given mass of rock that consists of interconnecting pores containing hydrocarbons and free water, including clay bound water (Deysse, 1988). The results of the 3-D porosity model are discussed later.

### Seismic Analysis

Since the seismic volume used for interpretation was recorded in two-way time (TWT), it is important to establish a relationship between the time domain of the seismic and the depth domain of the well logs. Synthetic seismograms were created by

generating an acoustic impedance (AI) log from DT and bulk density (RHOB) logs by the following formula:

$$\text{RHOB} \times \text{DT} = \text{AI} \qquad 3.4$$

Synthetic seismograms were created in nine wells in the study area (Figure 15), and were matched with extracted wavelets along the wellbore from the seismic volume. These wells were selected in order to get an accurate time-depth correlation across the 3-D survey. Depositional dip in the study area is oriented approximately NE-SW. Ties between the synthetic seismograms and the extracted wavelets were fairly accurate, which allowed for correlation between well tops picked in depth to their respective seismic reflections measured in TWT.

Four seismic horizons were interpreted in the 3-D survey. The Strawn Limestone underlies a thick section of Pennsylvanian shales, and has a high positive acoustic impedance value corresponding to a peak in seismic reflection data. This horizon was picked first because of its continuity throughout the survey provided for a general stratigraphic constraint through the entire survey. The top of the Cline Shale section corresponds to a high negative acoustic impedance value, resulting in a fairly continuous trough in the seismic data. This reflector is interpreted as the approximate Upper Pennsylvanian-Wolfcampian interface. The top Wolfcamp-base Leonard reflector also is fairly continuous throughout the survey, though it diminishes in amplitude and continuity moving depositionally downdip to the southwest. This interface is marked by

a trough, as high velocity detrital carbonates of the lower Leonardian form a sharp contact with the underlying Wolfcampian section of calcareous shale and carbonate detritus. The Wolfcamp section thins basinward onto the underlying Cline interval. Interpreted as the Leonardian-Guadalupian sequence boundary, the top of the Upper Spraberry Sand was picked in the survey as a seismic trough. Based on seismic and sequence stratigraphic principles of Vail et al. (1977), the Spraberry section represents a lowstand systems tract (LST) in the Midland Basin, and was used as an upper stratigraphic constraint for interpretation within the survey.

The Strawn Limestone, Upper Cline Shale, Wolfcamp Shale, and Upper Spraberry time horizons were initially interpreted along a 10-line by 10-trace spacing. Due to weak reflection qualities of the Wolfcamp Shale and Upper Cline horizons, additional interpretation was conducted along vertical slices oriented normal to depositional dip at 5-line spacing. An autopicking algorithm was then used to complete the horizon interpretation. The horizons were then checked for bad picks, reinterpreted, and converted to seismic surfaces. Horizontal time slices were used to identify downslope transport of detrital sediments based on reflection amplitude strength and geometry.

Seismic attributes are extensively used by industry to better characterize depositional patterns in the subsurface and predict reservoir occurrence. For this project, structural smoothing, variance, chaos, root mean squared (RMS) amplitude, relative acoustic impedance, Ant Tracking, and genetic inversion volumes were created in order to aid horizon and structural interpretation within the study area and to analyze



geomorphologic depositional patterns within the Lower Permian detrital carbonate interval.

Horizon/time slice interpretation and seismic facies analysis were conducted using a structurally smoothed seismic volume, in which seismic reflectors from the original amplitude volume are smoothed with a local averaging method (Figure 16). The “smoothed” 3-D seismic volume illustrates the carbonate platform transition from an Early to Middle Paleozoic ramp to a Late Paleozoic rimmed shelf. Seismic reflections of the Ordovician through Pennsylvanian tend to be fairly continuous and parallel, dipping subtly towards the southwest, typical of the carbonate ramp environment of the Early and Middle Paleozoic (Ward et al., 1986). Reflections begin to deviate from parallel in Upper Pennsylvanian through Wolfcampian units in the northeast area of the survey. Interpretations made from these reflection geometries indicate that the seismic survey is positioned along the Wolfcampian-Leonardian lower slope and basin. Overall topographic relief from the shallow shelf to deep basin is much higher by Lower Guadalupian time, and a dip section through the survey shows steep clinoforms that prograde westward into the Midland basin (Figure 17). Reflections show offlapping geometry along the base of the clinoforms and a toplapping signature along the upper part.

Structurally, the seismic survey is characterized by a few near vertical, low displacement faults, creating subtle drape structures with small amounts of displacement. Most of these faults terminate upwards into the Cline Shale, while a few displace

Wolfcampian-Leonardian strata. A few intraformational faults and drape structures also occur within the overlying Permian section of the study area.

A time slice through a genetic inversion attribute volume flattened along the interpreted Upper Wolfcamp time horizon reveals a basinward trending pattern of high acoustic impedance values that look similar to depositional geometries expected from detrital carbonate deposition (Figure 18). Time slices generated at similar time intervals through the structurally smoothed amplitude volume show reflection patterns that are typically discontinuous with variable amplitude strength. Primary reflection trends within the data are 1) northwest-southeast trend that correspond to Lower Permian depositional strike and 2) northeast-southwest trend that correspond to direction of depositional dip and most likely reflects depositional features in the seismic volume. Several lobate patterns are also identified within the amplitude volume and may correspond to the gross structure of debris flows in plan view.

Four seismic facies were identified and described (Table 2) within the Wolfcampian-Leonardian section. The Wolfcamp-Leonardian section consists mainly of subparallel, semicontinuous to discontinuous reflections. These reflections range in amplitude from high to low, and in some areas show reflection broadening. Facies 1, 2, and 3 all have parallel reflection configurations and continuous to semi-continuous reflection continuity. Whereas facies 2 has an onlapping relationship with underlying reflectors, facies 4 has a mounded reflection geometry characterized by a scoured lower reflector with subtle onlap of adjacent reflections. Facies 4 is interpreted as a potentially

thick, channelized debris flow or grain flow that was transported downslope during a mass wasting event.

In addition to the structurally smoothed volume, the RMS amplitude attribute volume was useful in providing additional stratigraphic interpretation (Figure 19). In particular, it appears that a correlation may exist between detrital carbonate thickness observed in well logs and a large amplitude response from the RMS amplitude volume. The dip section through the RMS amplitude volume (Figure 19) shows a pattern of high RMS amplitude response along the interpreted toe-of-slope and basinal position of the Lower Leonardian. This pattern of high amplitude response is also identified in the overlying Guadalupian section. A cross section was generated through four wells that penetrate the Lower Leonardian detrital interval and was compared to associated RMS amplitude responses (Figure 20). The cross section shows that 3 of 4 wells have thick detrital carbonate intervals and correspond to a large RMS amplitude value. Although the fourth well contains detrital intervals, it is thought that the individual intervals may not be of sufficient thickness to generate the strong amplitude response. Based on porosity data from well logs, a correlation between porous detrital carbonates and associated amplitude response is not proposed. Production data from these wells was not readily available, and therefore could not be used to strengthen this argument. An RMS amplitude extraction was performed along the interpreted Upper Wolfcamp time horizon (Figure 21). Results show a basinward trending pattern of high RMS amplitude values similar to those seen in the time slice from the genetic inversion attribute volume (Figure 18). Additionally, the RMS amplitude extraction indicates a large area of high

RMS amplitude values trending northwest towards the Powell Ranch Field area, an area historically known for its prolific hydrocarbon production from Leonardian detrital carbonates (Montgomery, 1996; and Mazzullo, 1997).

A seismic geobody from the Wolfcamp-Leonardian detrital carbonate section was extracted from the 3-D seismic survey (Figure 22) by applying an opacity filter that displayed only high RMS amplitude values. For this project, high RMS amplitude values in the Wolfcamp-Leonardian section were interpreted to correspond to thick detrital carbonate intervals. It is possible to create a more accurate 3-D facies model by using seismic geobodies extracted from seismic as additional constraint. Success with this approach assumes that the user has an understanding of lithofacies and their associated seismic response. With an accurate velocity model or depth converted seismic volume, geobodies can be converted to the depth domain and, in addition to existing well control, be used as additional stratigraphic constraint in creating a 3-D facies model. However, velocity modeling and seismic depth conversion is outside the focus of the project and was not performed.

### Three Dimensional Reservoir Modeling

By integrating physical rock descriptions, well log response, petrophysics, and seismic reflection data, a three dimensional model of the Wolfcampian-Leonardian detrital carbonate depositional system was constructed. Upscaling well logs involved assigning averaged discrete values and petrophysical values to cells in a 3-D grid that were penetrated by well logs (Petrel, 2010). This was done over the entire interval of interest, and the number of cells in the constructed 3-D grid was determined based on

available computing power and desired resolution. Resolution is dependent on the number of control points, or wells, that are used, as well as the number of cells used in the 3-D grids. Since structural deformation within the study area is limited to low displacement faults and drape structures, no faults were incorporated into the 3-D grids. Data analysis was performed on the upscaled values in order to define variograms necessary for populating the grids and to remove any trends present in the data. The best fit variograms were determined for each zone, and were forced to honor wellbore data.

Several different models were generated over the Wolfcamp-Leonard section in order to evaluate the validity of applying stochastic models over the specified study area. Two separate facies models were generated by upscaling 1) facies logs created by the TEM process and 2) GR values. A smaller section of the study area with dense well control was used to shorten processing time and to obtain a more accurate model.

For the lithofacies model (Figure 23), a Sequential Indicator Simulation (SIS) algorithm was applied to 161 wells in a four-zone grid with cell dimensions 500ft (x) x 500ft (y) x 10ft (z). The populated model gives geologically reasonable results in that it illustrates the general lithological differences between Lower Leonardian and Wolfcampian strata within the study area. The Lower Leonardian has a large concentration of detrital carbonate facies, with an interbedded siltstone facies that corresponds to the Dean Sand. The siltstone facies thins to the north based on the north-south transect in Figure 23. In the Wolfcampian interval, lithology changes to mostly basinal shale with fewer detrital carbonate intervals of which none are continuous. However, this model provides little information with respect to detrital carbonate facies

trends and distribution, for example. Sequence boundaries or traceable beds cannot be identified from the lithofacies model.

Gamma ray values from 201 wells were upscaled to a four-zone grid with cell dimensions 500ft (x) x 500ft (y) x 5ft (z) that was populated using a Gaussian Random Function Simulation (GRFS) algorithm (Figure 24). The model results from cell population seem reasonable within zones 2, 3, and 4, corresponding to the Dean Sand, sub-Dean (Leonardian), and Wolfcampian, respectively. Zone 1 (Wichita) is the least geologically viable. The north-south transect shows alternating sequences of high (shale) and low (carbonate) GR values within the Wolfcampian section, interpreted as depositional sequences, most likely third-order sequences (Flamm, 2008). The Lower Leonardian section shows the significant increase in detrital carbonate deposition within the study area. This zone is overlaid by the high GR Dean Sand, which thins to the north up onto the slope. The east-west transect shows a similar result, with identifiable Wolfcampian sequences and a thick section of Lower Leonardian detrital carbonate. In this transect, the overall thickness of the sub-Dean detrital interval decreases basinward, with several isolated detrital intervals farther basinward.

PHIT values from 161 wells also were upscaled and populated into a two-zone grid with cell dimensions of 500ft (x) x 500ft (y) x 5ft (z). The resultant porosity model (Figure 25) was generated over a smaller section of the study area than the facies model. The Wolfcampian and sub-Dean detrital intervals are easily identifiable based on the contrast in porosity values. Based on results from the formation evaluation, it is determined that low PHIT values (less than 0.06) correspond to detrital carbonate

intervals, whereas high PHIT values (greater than 0.06) are most likely basinal shale. Of the two zones that were modeled, the sub-Dean interval looks the most geologically reasonable. Depositional sequences identified in the facies models are not readily identifiable within the porosity model. A zone of high porosity is observed within the sub-Dean interval along the north-south transect, with porosity values exceeding 0.16. After comparing this zone to the same interval from the facies model, it was determined that this zone of high porosity corresponds to a porous detrital carbonate interval. Since PHIT values are affected by clay bound water within the basinal shale facies, porosity is overestimated. Therefore, since porosity values calculated within porous carbonate facies intervals are often similar to values seen within the basinal shale facies, it is difficult to distinguish porous carbonate facies from adjacent basinal shale facies within the porosity model without the aid of the facies model or a GR log.

## CHAPTER IV

### DISCUSSION

Seismic, well log, and subsurface core data from the Wolfcampian-Leonardian section of the eastern Midland Basin was integrated into a series of three dimensional models in order to provide a more comprehensive understanding of the subsurface in order to characterize the stratigraphy of this area. Some of the interpretations discussed in the following sections are based on previous studies of other detrital carbonate outcrops, as well as outcrop studies of coeval rocks deposited farther west in the Delaware Basin (e.g., Crevello and Schlager, 1980; Cook and Mullins, 1983; Playton and Kerans, 2002).

#### Proposed Depositional Models

Based on seismic and well log interpretations of the Lower Permian strata within the study area, the Wolfcampian interval is a mud-dominated depositional environment consisting of basinal shales and mudstones interbedded with skeletal wackestone-packstone turbidites and a few discontinuous grain flows and debris flows. The overlying detrital carbonate interval of the Leonardian section best fits the grain-dominated *detrital apron* depositional model in which shelf margin derived carbonate material is transported and accumulates downslope, forming a thick, strike-continuous grainstone-rudstone apron of detritus that onlaps the slope and thins basinward (Mullins and Cook, 1986; and Playton et al., 2010). This model suggests that detrital aprons form primarily as a result of line sourced detrital transport and deposition via offshelf



transport mechanisms such as wave action, storms, and tidal flow (Playton et al., 2010). Mazzullo (1997) argues in favor of the *base-of-slope apron* model, stating that the Early Permian detrital apron in Glasscock County is located several miles basinward of the contiguous shelf edge, resulting in a bypass zone along the slope that separates the detrital apron from the shelf edge, and that detritus was transported downslope via submarine canyons. Conversely, the *slope apron* model argues that facies grade shelfward into platform-margin facies without a bypass zone (Mullins and Cook, 1986). Observations from this study seem to favor the *slope apron* model, since no significant evidence of a bypass zone was observed during well correlation, and the calculated slope gradient measured from well tops is relatively subtle at 4-5°. Although gullies and submarine canyons were not identified within the seismic dataset, the seismic survey is positioned along the lower slope and basinal regions with respect to Wolfcampian-Leonardian time, possibly westward of any noticeable bypass features.

The compositional and geometrical characteristics described in Wolfcampian-Leonardian section reflect a period in which the accretionary margin of the eastern Midland Basin was transitioning from a ramp to a rimmed shelf. No significant progradational clinoforms were identified in the Lower Permian strata from seismic, but a substantial increase in paleobathymetric relief is evident from well logs.

#### Timing of Deposition/Mechanisms for Transport

Determining the relative timing of detrital apron formation in Glasscock County was not clear from core descriptions or from the seismic survey. Arguments covering highstand and/or lowstand shedding of detrital carbonates are numerous. A lowstand

shedding model is based on the observation of lowstand units identified from seismic reflection data (Leary and Feeley, 1991) and the interpretation of an inverted acoustic impedance volume (Flamm, 2008). Highstand shedding of platform derived carbonate sediments is supported by extensive petrographic and geochemical studies conducted on cores (Mazzullo and Reid, 1989; Mazzullo, 1994; and Mazzullo, 1997). Evidence from outcrops in the Sierra Diablo Mountains indicates the formation of a detrital apron during highstand accommodation settings along a tectonically active late Wolfcampian shelf margin (Playton and Kerans, 2002). Early Permian eustatic curves (Mazzullo, 1995; and Sarg et al., 1999) for this study area show that detrital carbonate deposition may have occurred during sea level highstand. Cores in this study show gravity flow deposits interfingering in basinal settings with shale, rather than sandstones and silts typical of lowstand sedimentation. Deposition of the immediately overlying Dean Sand occurred during sea level lowstand (Mazzullo, 1997). Sediment gravity flow deposition, given the right circumstances, can occur at any time (Flamm, 2008) as a result of mechanisms aside from sea level position. Three proposed mechanisms of shelf failure and subsequent mass transport of shelf derived detritus include subaerial exposure and erosion of the shelf edge, oversteepening the shelf edge due to a vertical aggradation, and shelf edge failure triggered by tectonism (Mazzullo and Reid, 1987). Tectonic activity related to continental collision occurred throughout the Wolfcampian (Yang and Dorobek, 1995). Seismic data in the study area reveals a few small, low displacement intraformational faults occurring within the Wolfcampian-Leonardian section. Since the seismic data in this study is along the lower slope and basinal regions, it cannot be

determined if mass wasting during the Wolfcampian-Leonardian are related to tectonism along the shelf edge. However, evidence from well log correlation suggests that vertical aggradation of the shelf margin could have led to oversteepening and subsequent failure.

The transport of large amounts of shallow water detritus along a relatively gentle slope is problematic. Generation of grain flows usually require slope gradients of approximately 30° (Lowe 1976b; Middleton and Hampton, 1976; Cook, 1983), far more than the calculated Wolfcampian-Lower Leonardian slope gradients of 4-5°. Thus, it may be best to classify the grain flow facies described in this study as a density-modified grain flow (Lowe, 1976), where the grain flow is initiated and able to be transported down a more gentle gradient slope by friction reduction within the grain flow itself or by an external force, such as sustained downward shear of surface currents (Flamm, 2008; Cook 1983). Debris flows, or cohesive flows (Lowe 1976b), can be transported in a similar fashion, but are initiated by gravitational collapse and in some instances have very large individual runout distances (Crevello and Schlager, 1980).

#### Seismic Resolution of Detrital Carbonate Reservoirs

The Wolfcampian section is interpreted to consist mainly of basinal shale and thin grain flows and distal turbidites, whereas the Lower Leonardian section contains much thicker detrital carbonate debris flows and grain flows, increasing in concentration eastward. However, individual mass wasting events are difficult to identify from both the seismic volume and the generated attribute volumes. Assuming that seismic resolution is one-fourth of a wavelength, the limit of vertical resolution ( $h$ ) for the seismic data within the Wolfcampian-Leonardian section was determined at the Garden

City #1 using a dominant frequency ( $f$ ) of 32 Hz, an interval thickness ( $\Delta z$ ) of 1002 ft (305 m), and a one-way time ( $t$ ) of 0.05977 seconds.

$$\text{Vertical resolution } (h) = \frac{1}{4} ((\Delta z / t) / (f)) = 131 \text{ ft (40 m)} \quad 4.1$$

For individual flows to be detectable from seismic ( $1/8 \lambda$ ), the thickness of the debris flow / grain flow would have to be approximately 65 ft (20 m) thick. The limit of vertical resolution is dependent upon several factors, including signal-to-noise ratio, rock velocity, and heterogeneity within the interval of interest (Taner, 1997). The thickest detrital interval identified from well logs in the Wolfcampian section was approximately 80 ft (24 m). Therefore, even under ideal conditions (low noise and attenuation levels), it is unlikely that all individual mass wasting events could be resolved in the Wolfcampian section from the seismic volume. Although individual flows may not be resolvable, resolution of a detrital interval could be achieved if several flows were stacked vertically and exceeded the minimum thickness for vertical resolution. The thicker detrital section observed in well logs in the Lower Leonardian section should be resolvable, and may be represented by mounded, discontinuous seismic reflectors that characterize the Leonardian section in the central and eastern part of the study area (Figure 17). However, flows in seismic represent a detrital interval consisting of multiple, amalgamated mass wasting events as opposed to individual flows.

### Viability of Utilizing 3-D Reservoir Modeling

The accuracy of a 3-D model is dependent upon the amount of input data constraints (i.e., well control) and the overall quality of the conditioned data.

Uncertainty involved within a model can only be decreased by increasing the amount and quality of the input data, and the addition of data to a model is likely to produce different results.

The application of 3-D facies and porosity models within the study area yielded both promising and disappointing results. These models were run over a small portion of the study area where well control was densest. The facies models derived from upscaled 1) GR and 2) lithofacies logs are useful in illustrating the general lithological composition of Early Permian strata, identifying potential sequence boundaries within the Wolfcampian section, and determining the relative distribution of detrital carbonate sediments within the Lower Leonardian interval. Of the four zones that compose the facies models, acceptable results were achieved in three of the four zones. The porosity model derived from upscaled PHIT values was less valuable in terms of being able to make geological predictions. Only 1 of the 2 zones modeled showed any geological sense, which is most likely due to the fact that there was less data constraining the PHIT model. A distinction between basinal shales and “tight” detrital carbonates could be identified, but a distinction could not be made between porous detrital carbonate intervals and basinal shales due to the similarity in upscaled PHIT values.

## CHAPTER V

### CONCLUSIONS

#### Summary

Integration of core, well log, and 3-D seismic data allowed for a comprehensive analysis of the Early Permian strata in the Eastern Midland Basin. Detrital carbonate deposits within the Wolfcampian-Leonardian slope and basin sections consist of distal turbidites, modified grain flows, and debris flows, which form a *detrital apron* that interfingers with basinal shale. It was determined that detrital carbonate deposition during the Early Leonardian occurred along a low gradient slope (4-5°). It is interpreted that sediment gravity flows during this period most likely occurred during sea level highstand, and may have resulted from Wolfcampian tectonism and local failure caused by an oversteepened shelf margin, although other alternatives are considered. The generation of seismic attribute volumes aided greatly in horizon interpretation and seismic facies analysis of the Early Permian strata. The generation of an RMS amplitude attribute volume revealed depositional trends within the Wolfcampian-Leonardian, and was used to establish a potential correlation between detrital carbonate thickness and RMS amplitude response. Although the entire detrital carbonate interval is observed in the seismic reflection data, it was determined that the calculated limit of vertical seismic resolution for the data exceeded the cumulative thickness of most individual detrital carbonate intervals within the study area. The application of 3-D models within the study area was useful in reinforcing the argument of a *detrital apron* depositional model,

but was determined to be better suited to areas with more abundant and better conditioned input data.

## REFERENCES

- Asquith, G., D. Krygowski, 2004, Second Edition: Basic Well Log Analysis. AAPG Methods in Exploration Series, n. 16, 224 p.
- Atchley, S.C., Kozar, M.G., and Yost, L., 1999, A predictive model for reservoir distribution in the Permian (Leonardian) Clear Fork and Glorieta formations, Robertson field area, west Texas: AAPG Bulletin, v. 83, p. 1031– 1056.
- Cook, H. E. and Enos, P., 1977, Deep-water Carbonate Environments. Society of Economic Paleontologists and Mineralogists Special Publication 25, 336 p.
- Cook, H.E., 1983, Sedimentology of some allochthonous deepwater carbonate reservoirs, Lower Permian, West Texas: Carbonate debris sheets, aprons, or submarine fans?: AAPG Bulletin, v. 63, p. 442.
- Cook, H.E., and Mullins, H.T., 1983, Basin margin environment, *in* P. Scholle, D. Bebout, and C. Moore eds., Carbonate Depositional Environments: American Association of Petroleum Geologists Memoir 33, p. 539- 618.
- Crevello, P.D., and Schlager, W., 1980, Carbonate debris sheets and turbidites, Exuma Sound, Bahamas: Journal of Sedimentary Petrology, v. 50, p. 1121-1147.
- Dewan, J., 1983, Essentials of Modern Open-Hole Log Interpretation: Tulsa, Oklahoma, PennWell Publishing Company, 361 p.
- Dunham, R.J., 1962, Classification of Carbonate Rocks According to Depositional Texture, AAPG Memoir, 1, p. 108-121.
- Dutton, S.P, Kim, E.M., Broadhead, R.F., Raatz, W.D., Breton, C.L., Ruppel, S.C, and Kerans, C., 2005, Play analysis and leading-edge oil-reservoir development methods in the Permian basin: Increased recovery through advanced technologies, AAPG Bulletin, v. 89, no. 5, p. 553–576.
- Embry, A. and Klovan, J.E., 1971, A late Devonian Reef Tract on Northeastern Banks Island, Northwest Territories, Bulletin of Canadian Petroleum Geologists, 19, p. 730-781.
- Flamm, D.S., 2008, Wolfcampian Development of the Nose of the Eastern Shelf of the Midland Basin, Glasscock, Sterling, and Reagan Counties, Texas: Unpublished M.S. thesis, Brigham Young University.
- Glover, P.W.J., 2000, Petrophysics, University of Laval Course Notes, 281 p.
- Heysse, D., 1983, Open Hole Log Analysis and Formation Evaluation, Halliburton Logging Service, Houston, Texas, USA.
- Hobson, J. P., Jr., C. D. Caldwell, and D. E Toomey, 1985b, Early Permian deep-water allochthonous limestone facies and reservoir, West Texas: AAPG Bulletin, v. 69, p. 2130-2147.



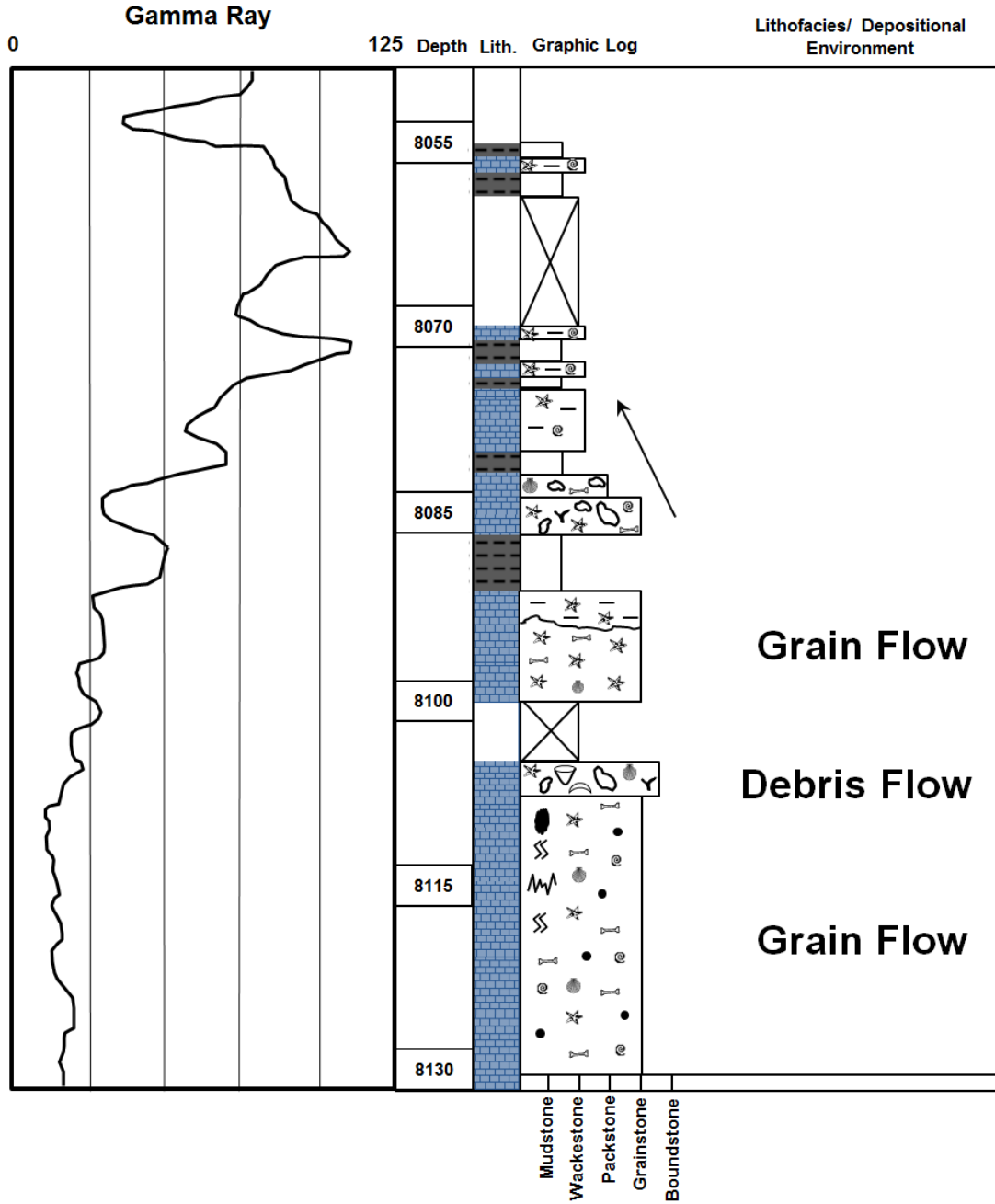
- Horak, R. L., 1985, Tectonic and hydrocarbon maturation history in the Permian basin: *Oil & Gas Journal*, May 27, v. 83, no. 21, p. 124– 129.
- Larionov, V.V., 1969, *Borehole Radiometry*: Moscow, U.S.S.R., Nedra.
- Leary, D.A., and Feeley, M.H., 1991. Seismic Expression and Sedimentologic Characteristics of a Permian (Wolfcampian) Carbonate Submarine Fan, Midland Basin, West Texas, *in* P. Weimer and M.H. Link, eds., *Seismic Facies and Sedimentary Processes of Submarine Fans and Turbidite Systems*, Springer-Verlag, New York, p. 303-315.
- Mazuingue-Desailly, V.P.G., 2004, *Assessing the Influence of Diagenesis on Reservoir Quality: Happy Spraberry Field, Garza County, Texas*: Unpublished M.S. thesis, Texas A&M University.
- Mazzullo, S.J., 1994c, Lithification and Porosity Evolution in Permian Periplatform Limestones, Midland Basin, Texas; *Carbonates and Evaporites*, v. 9, p. 151-171.
- Mazzullo, S.J., 1995, Permian Stratigraphy and Facies, Permian Basin (Texas-New Mexico) and adjoining areas in the Midcontinent United States, *in* P.A. Scholle, T.M. Peryt, and D.S. Ulmer-Scholle, eds., *The Permian of Northern Pangea*, v. 2, *Sedimentary Basins and Economic Resources*; Springer-Verlag, p. 41-60.
- Mazzullo, S.J., 1997, *Essential Elements of Stratigraphic Exploration Plays in Ordovician to Lower Permian Carbonates in the Midland Basin and on the Eastern Shelf*, SAC Press, Wichita, Kansas, 76 p.
- Mazzullo, S.J., and Harris, P.M., 1991, An overview of dissolution porosity development in the deep-burial environment, with examples from carbonate reservoirs in the Permian Basin, *in* M. Candelaria, ed., *Permian Basin Plays, Tomorrow's Technology Today*; WTGS, Publication 91-89, p. 125-138.
- Mazzullo, S.J., and Reid, A.M., 1987, Basinal Lower Permian Facies, Permian Basin: Part II- Depositional setting and reservoir facies of Wolfcampian-Leonardian basinal carbonates; *WTGS Bulletin*, v. 26, no. 8, p. 5-10.
- Montgomery, S.L., 1996, Permian "Wolfcamp" Limestone Reservoirs: Powell Ranch Field, Eastern Midland Basin, *AAPG Bulletin*, v. 80, no. 9, p.1349-1365.
- Mullins, H.T., and Cook, H.E., 1986, Carbonate Apron Models: Alternatives to the Submarine Fan Model for Paleoenvironmental Analysis and Hydrocarbon Exploration, *Sedimentary Geology*, v. 48, p. 37-79
- Mullins, H.T., and Cook, H.E., 1983,
- Playton, T.E., and Kerans, C., 2002, Slope and Toe-of-Slope Deposits Shed from a Late Wolfcampian Tectonically Active Carbonate Ramp Margin, *GCAGS Transactions*, v. 52, p. 811-820.

- Playton, T.E., Janson, X., and Kerans, C., 2010, Carbonate Slopes, *in* N.P. James and R.W. Dalrymple, eds., *Facies Models 4*, Series No. 4, Geological Association of Canada, p. 449-476.
- Sarg, J.F., Markello, J.R., and Weber, L.J., 1999, The second-order cycle, carbonate-platform growth, and reservoir, source, and trap prediction, *in* Harris, P.M., Simo, J.A., and Saller, A.H., eds., 1999. *Advances in Carbonate Sequence Stratigraphy: Application to Reservoirs, Outcrops, and Models*, Soc. Econ. Paleontol. Mineral. Special Publication, 62, p. 1-24.
- Schlumberger, 2010, *Petrel 2010 Property Modeling Manual*, Norway, 437 p.
- Schlumberger, 2010, *Petrel 2010 Seismic Visualization and Interpretation Manual*, Norway, 482 p.
- Stoudt, E.L., 1998, *Productive Carbonate Debris Flows (Resedimented Carbonates) from Leonardian Deposits of the Eastern Midland Basin, Glasscock County, Texas*, West Texas Geological Society Publications, 38 p.
- Schlager, W., Reijmer, J.J.G., and Droxler, A., 1994, Highstand Shedding of Carbonate Platforms, *Journal of Sedimentary Research*, v. B64, no. 3, p. 270-281.
- Tai, Po-Ching, 2000, Controlling Factors on the Development of Late Pennsylvanian-Leonardian Carbonate Platform Margins Around the Midland Permian Basin, West Texas, *AAPG Bulletin*, v. 84, no. 11, p. 1860–1882.
- Taner, M. T., 1997, Seismic data processing flow in areas of shallow carbonates, *in* K. J. Marfurt ed., *Carbonate Seismology*, SEG, p. 223-279.
- Vail, P.R., Todd, R.G., Sangree, J.B., 1977, Seismic Stratigraphy and Global Changes of Sea Level, Part 5: Chronostratigraphic Significance of Seismic Reflections, *in* Payton, C.E. ed., *Seismic Stratigraphy- Applications to Hydrocarbon Exploration: AAPG Memoir 26*, p. 99-116.
- Ward, R.F., Kendall, C.G.ST.C., Harris, P.M., 1986, Upper Permian (Guadalupian) Facies and their Association with Hydrocarbons-Permian Basin, West Texas and New Mexico, *AAPG Bulletin*, v. 70, n. 3, p. 239-262.
- Yang, K.M., and S.L. Dorobek, 1995, The Permian Basin of West Texas and New Mexico: tectonic history of a “composite” foreland basin and its effect on stratigraphic development, *in* S.L.Dorobek and G.M. Ross, eds., *Stratigraphic Evolution of Foreland Basins: SEPM Special Publication 52*, p. 147-172.

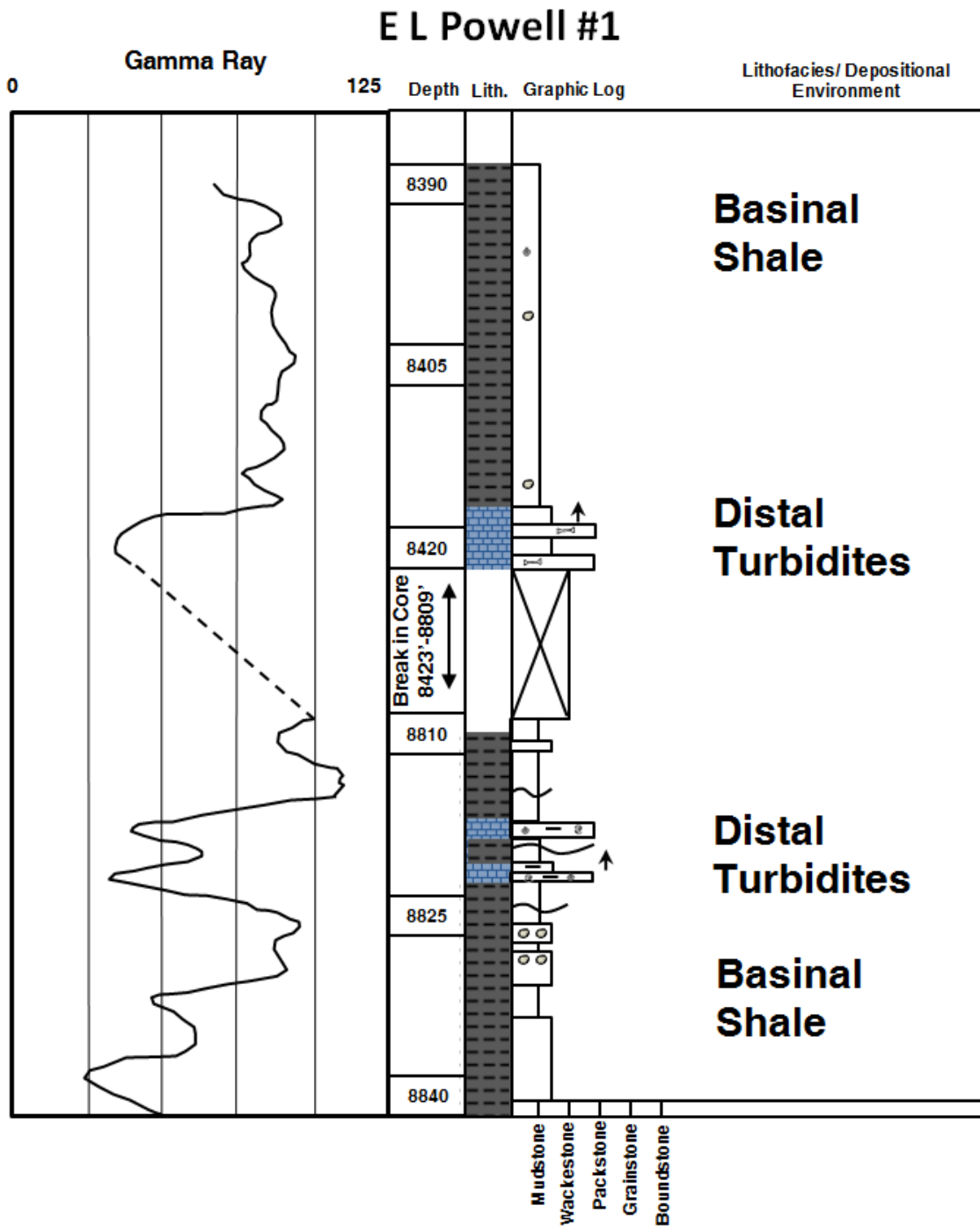
APPENDIX A

ADDITIONAL CORE DESCRIPTION

**E L Powell #1**

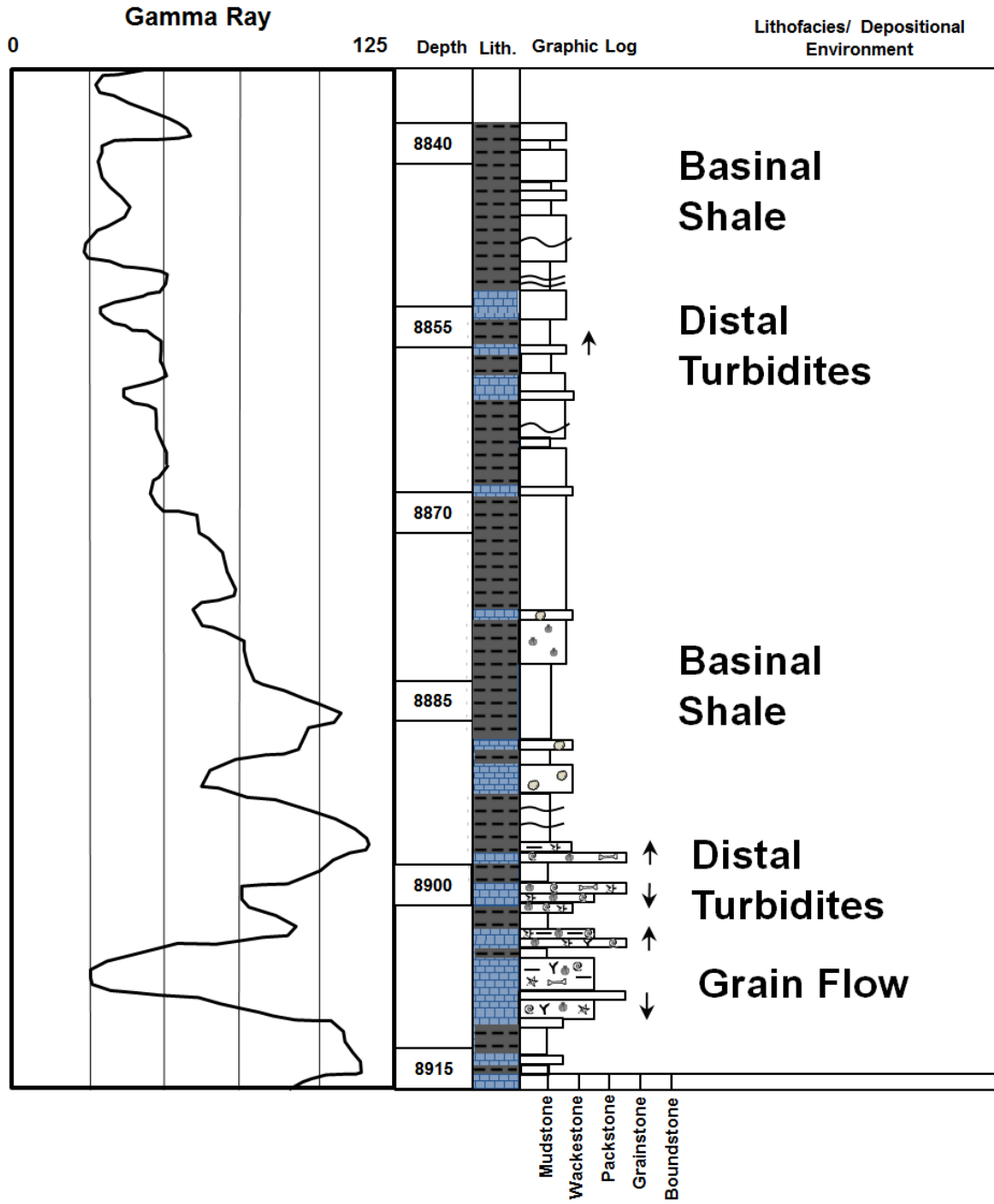


E L Powell #1 described core from 8055-8130 ft with associated gamma ray log.



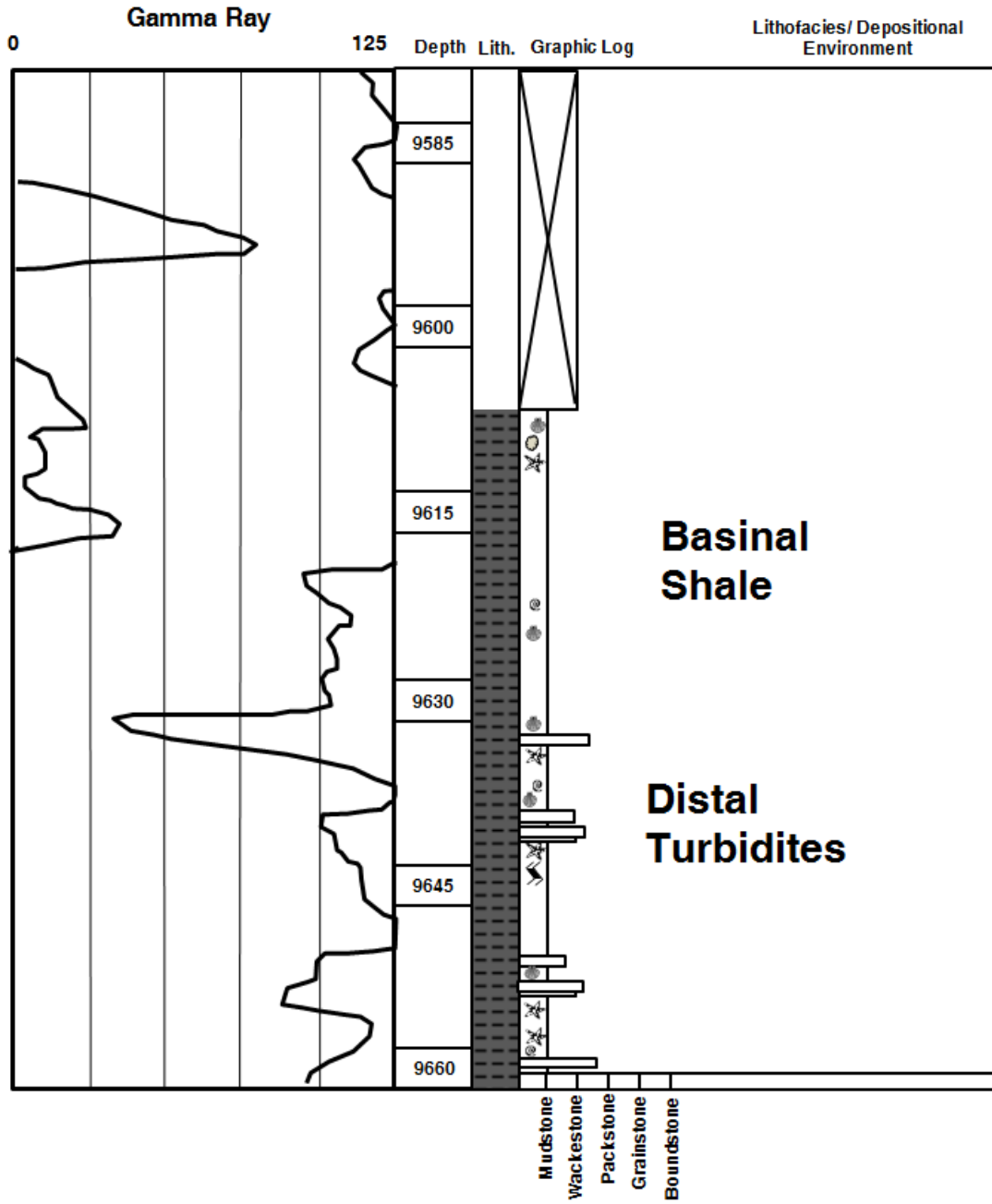
E L Powell #1 described core from 8390-8840 ft with associated gamma ray log.

# E L Powell #1



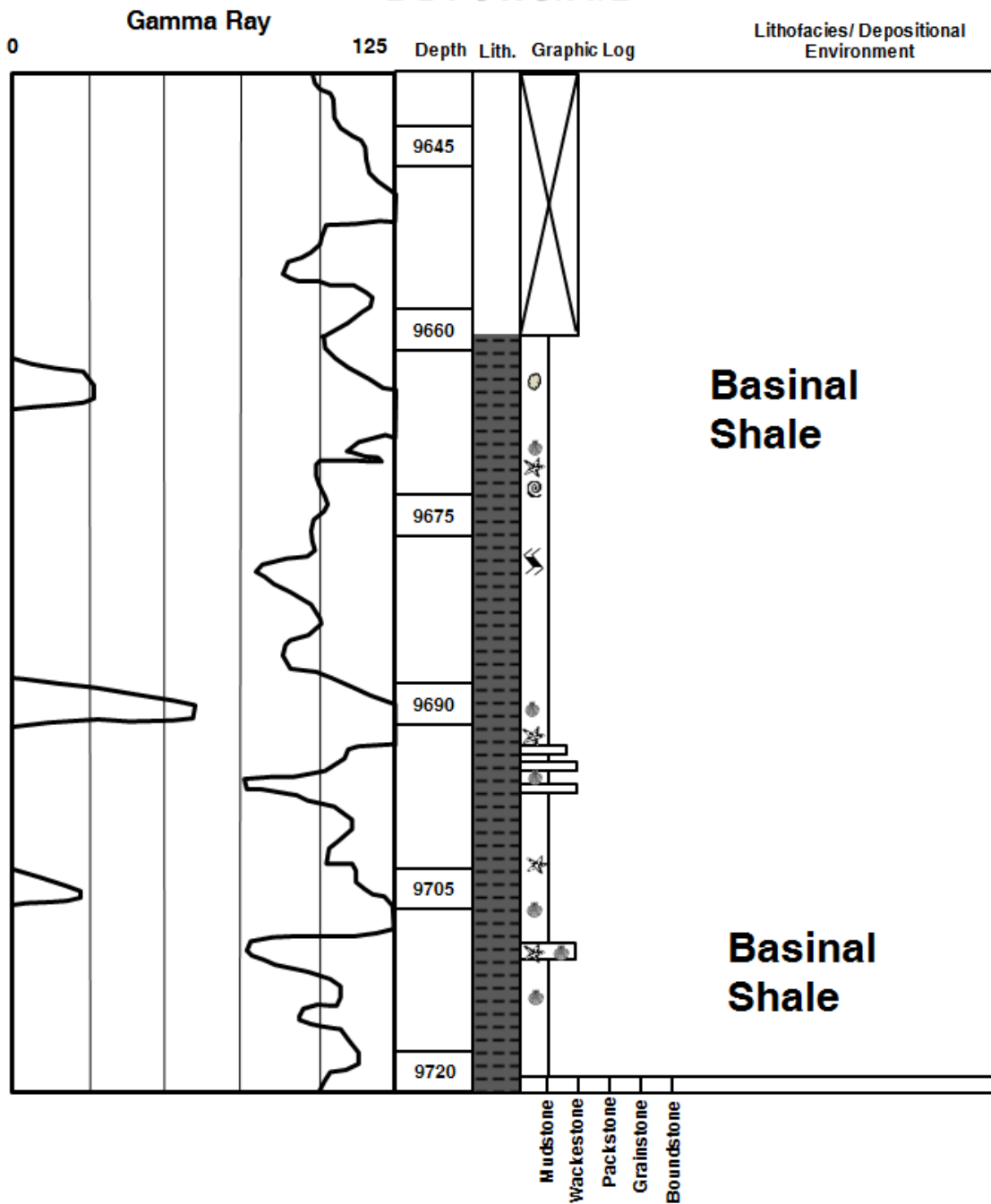
E L Powell #1 described core from 8840-8915 ft with associated gamma ray log.

# E L Powell #1





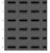


















E L Powell #1 described core from 9585-9660 ft with associated gamma ray log.

# E L Powell #1



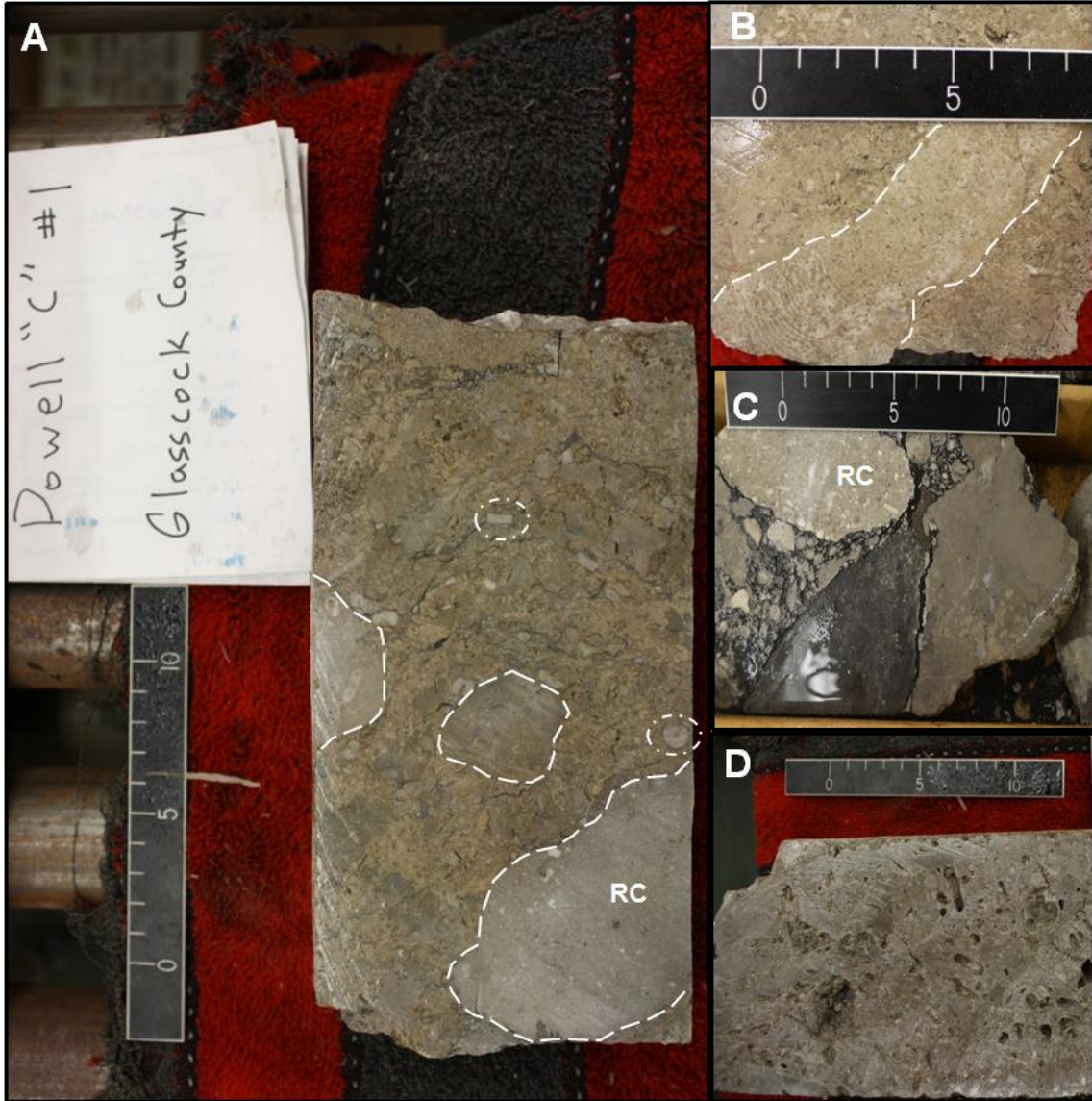
E L Powell #1 described core from 9645-9720 ft with associated gamma ray log.

Core Description Legend			
Lithology	Grain Types	Sedimentary Structures	Diagenetic Features
 Limestone	 Brachiopod	 Erosional Surface	 Vertical Fracture (filled)
 Shale	 <u>Bryozoan</u>	 Geopetal Structure	 Vertical Fracture (open)
	 Crinoid	 Graded Bedding	 Vug (filled)
	 Fusulinid	 Thin bed/ lamination	 <u>Stylolite</u>
	 Nodule		
	 Pellet/ <u>Peloid</u>		
	 Phylloid Algae		
	 Reefal Clast		
	 Shale Matrix		
	 Sponge		
	 Undifferentiated Skeletal Fragment		

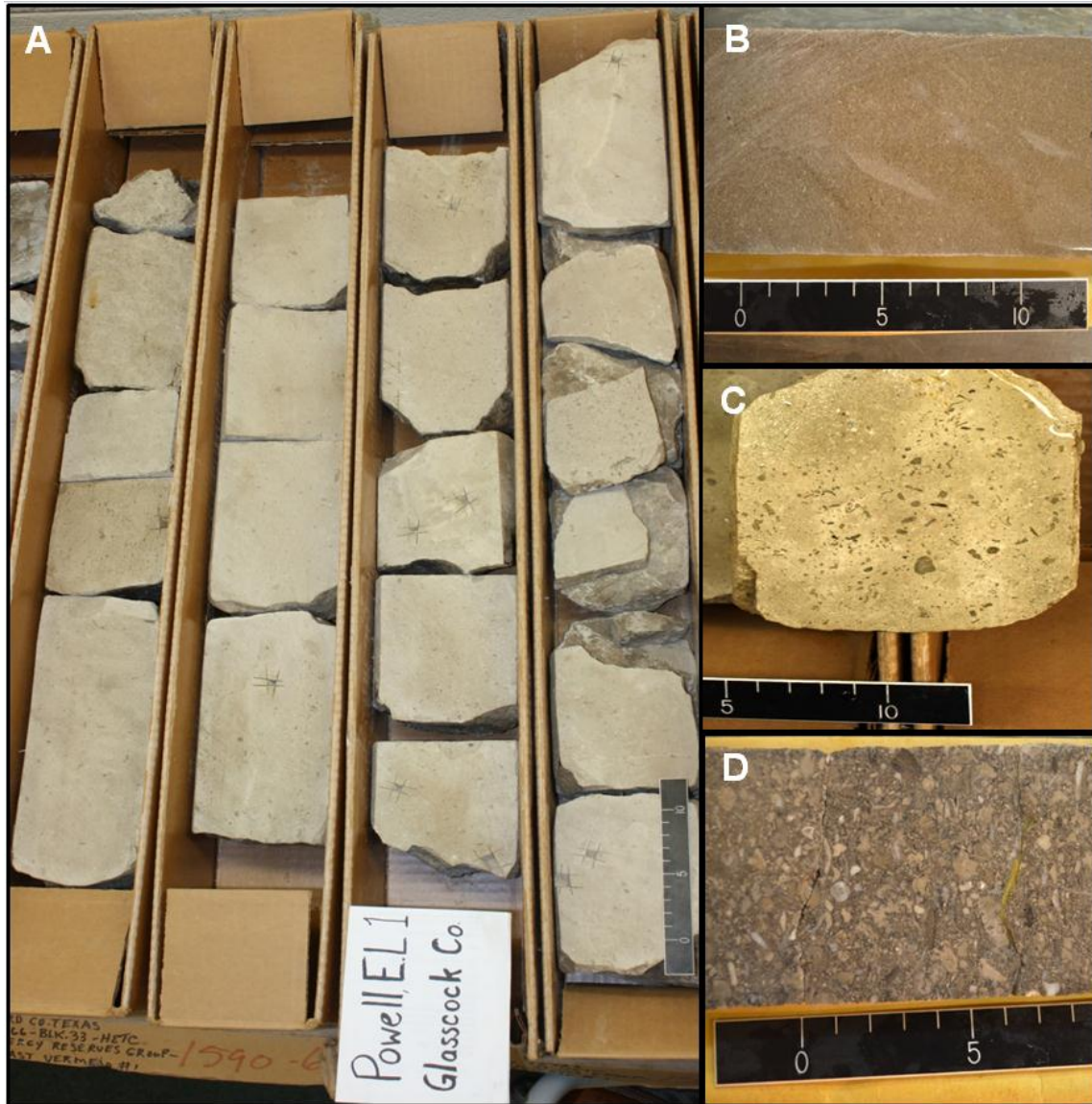
Core description legend used for this study.



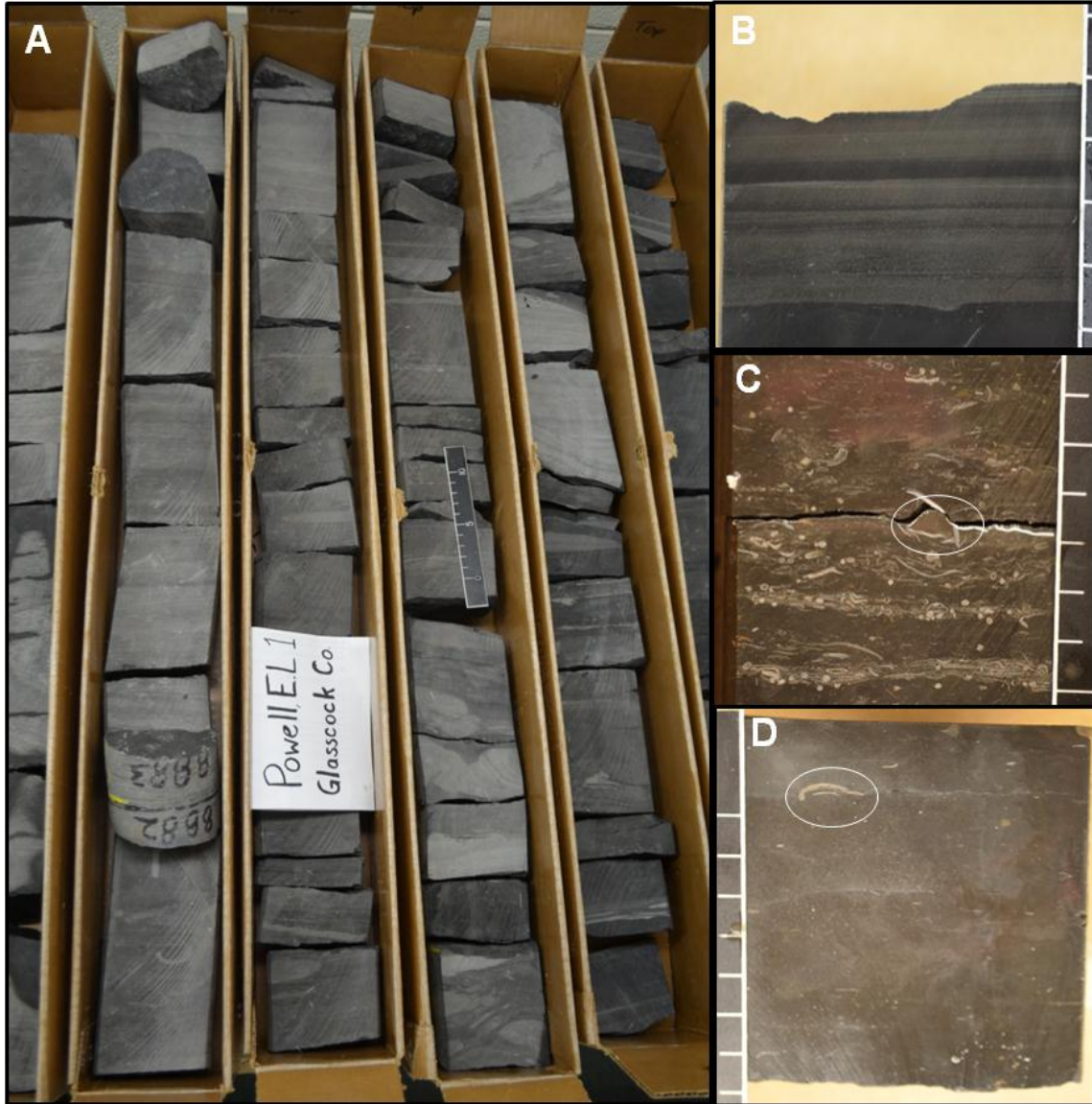
APPENDIX B  
CORE PHOTOGRAPHS



Core photographs taken from the Powell "C" #1 well illustrating the *debris flow* facies. Note A) large reefal clasts and crinoid fragments (outlined in white) and B) phylloid algae fragment. C) Clast supported conglomerate with a dark *basinal shale* matrix. D) Single lithoclast showing large amounts of dissolution porosity.



Core photographs taken from the E.L. Powell #1 (A,C) and J.W. Cox #1 (B, D) wells illustrating the *grain flow* facies. The interpreted *grain flow* facies consists of carbonate sand and crinoid/pelletal-skeletal grainstone. Visible interparticle porosity is observed.



Core photographs taken from the E.L. Powell #1 well showing the *basinal shale* facies. Thin calcisiltstones (B) and skeletal-rich packstones with occasional muddy intraclasts (C) are observed. Note the large brachiopod fragment outlined in the white circle in (D).

APPENDIX C

FIGURES

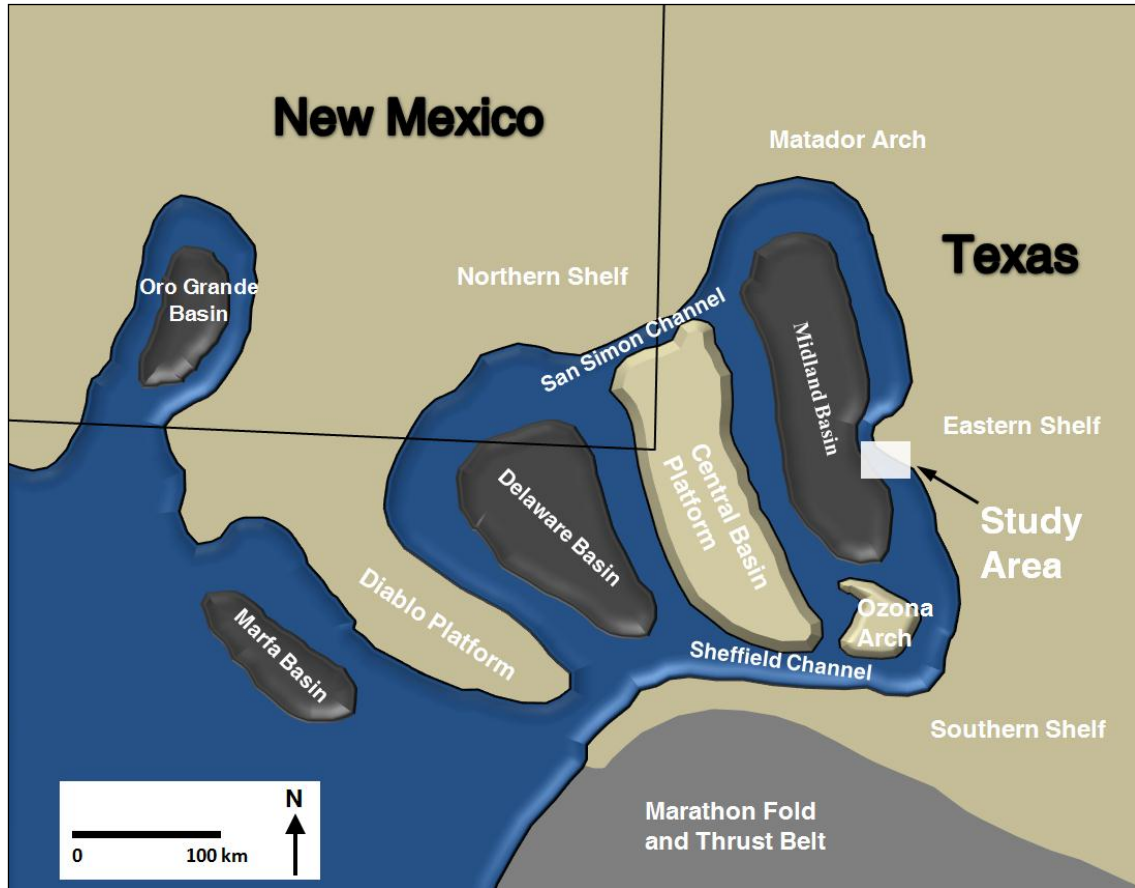
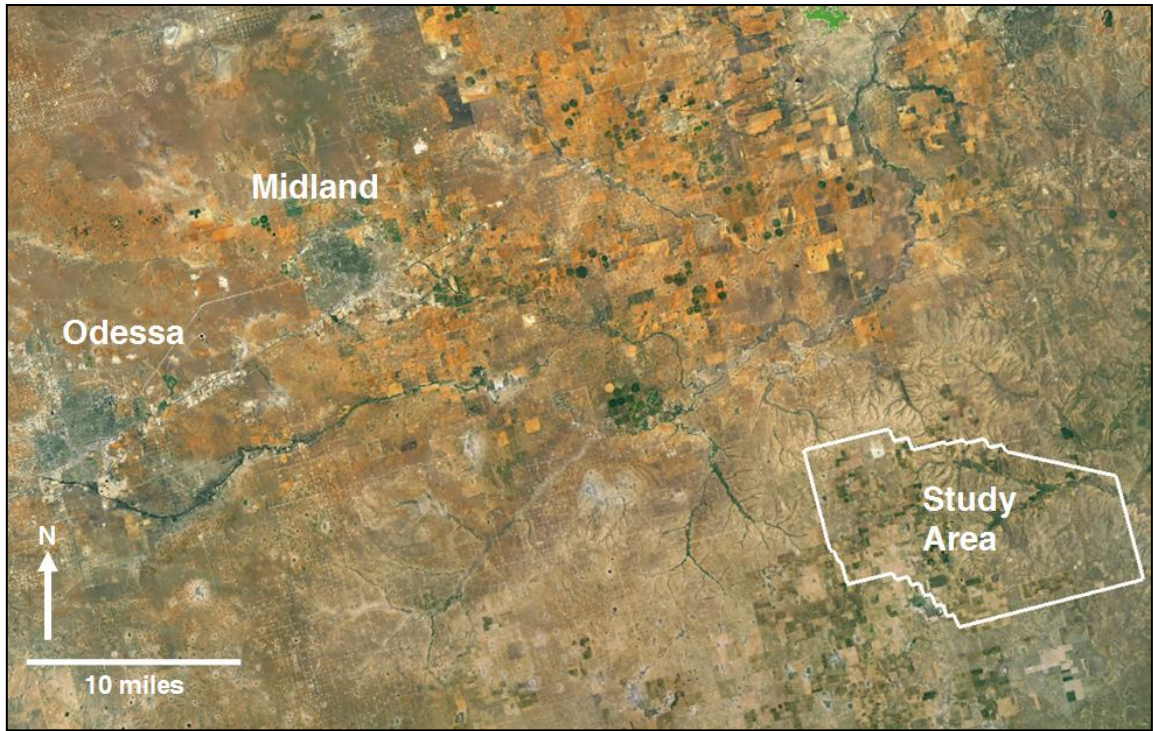


Figure 1: Permian Basin Regional Map. (Modified from Flamm, 2008).

System	Epoch	Midland Basin	Eastern Shelf	
Permian	Guadalupian	Artesia Group		
		San Andres		
		Glorieta	San Angelo	
	Leonardian	Clearfork	Clearfork	Wichita Group
		Spraberry	Wichita Group	
		Wichita Detrital		
		Dean Sand		
		Sub-Dean Detrital		
	Wolfcampian	Wolfcamp		
	Upper Pennsylvanian	Virgilian	Cisco	
Missourian		Canyon		
Desmoinesian		Strawn		

This Study

Figure 2: Stratigraphic Column of Desmoinesian-Guadalupian strata in Eastern Midland Basin.



**Figure 3: Satellite image of the geographical location of the study area.**

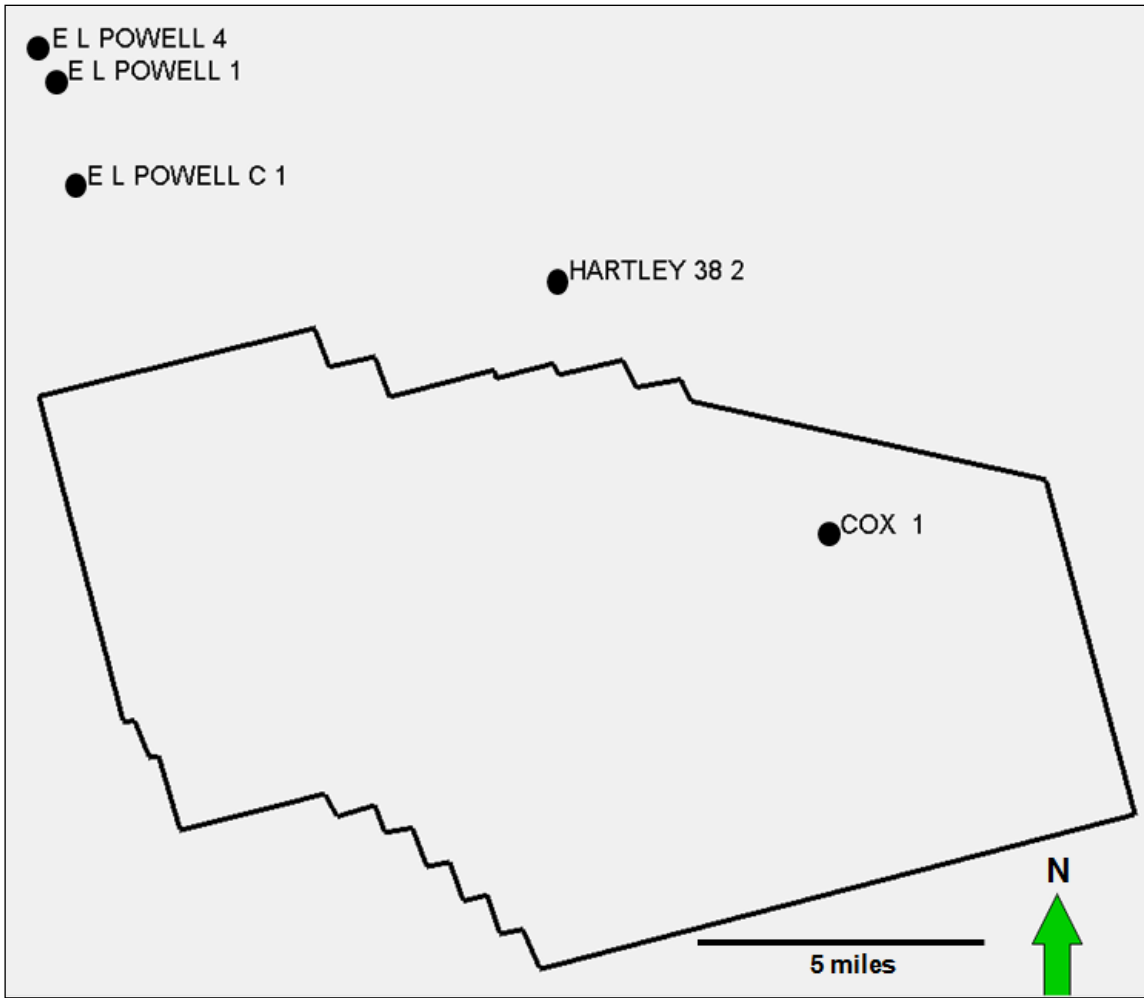


Figure 4: Location of cores described for the project with respect to the 3-D seismic survey location.

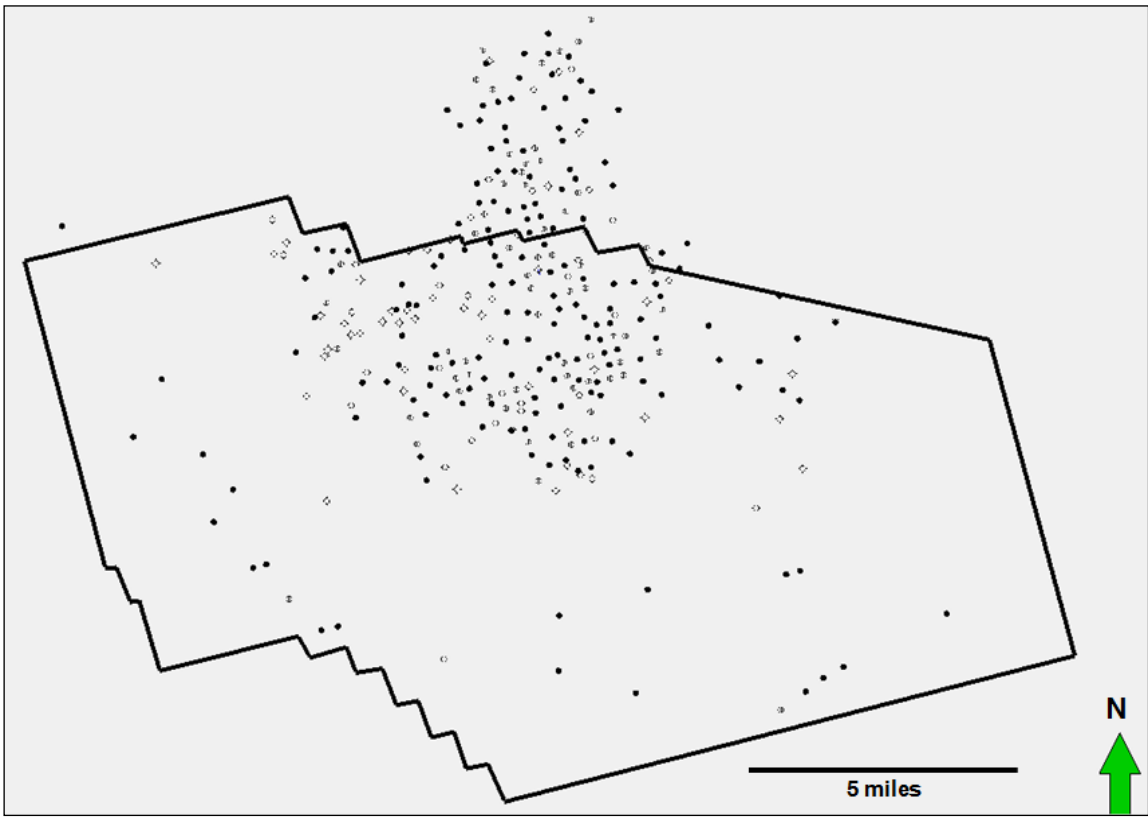
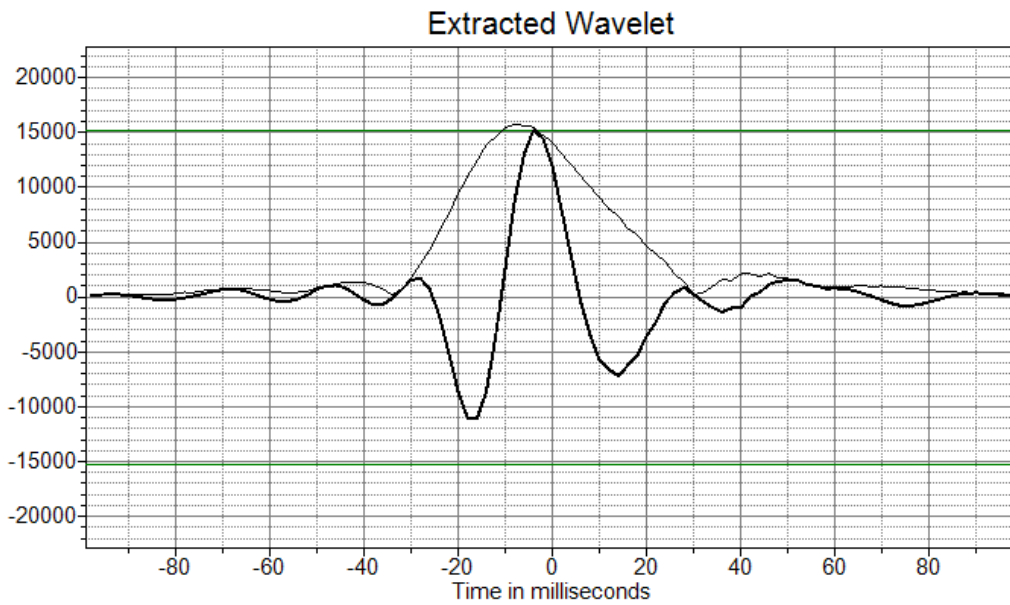
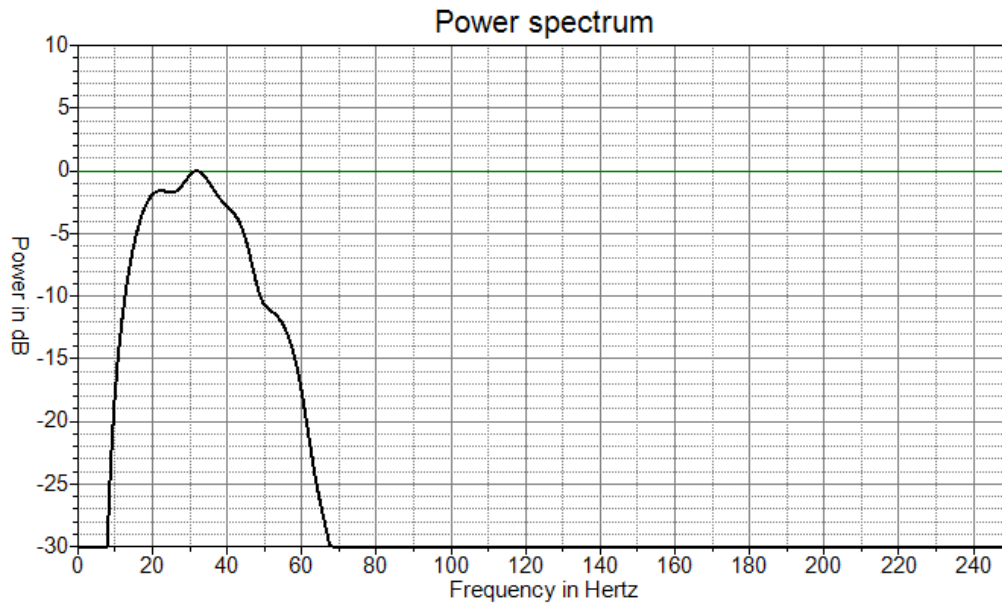


Figure 5: Extent of well coverage used for the study.





**Figure 6: Extracted wavelet and power spectrum taken from the Garden City #1.**

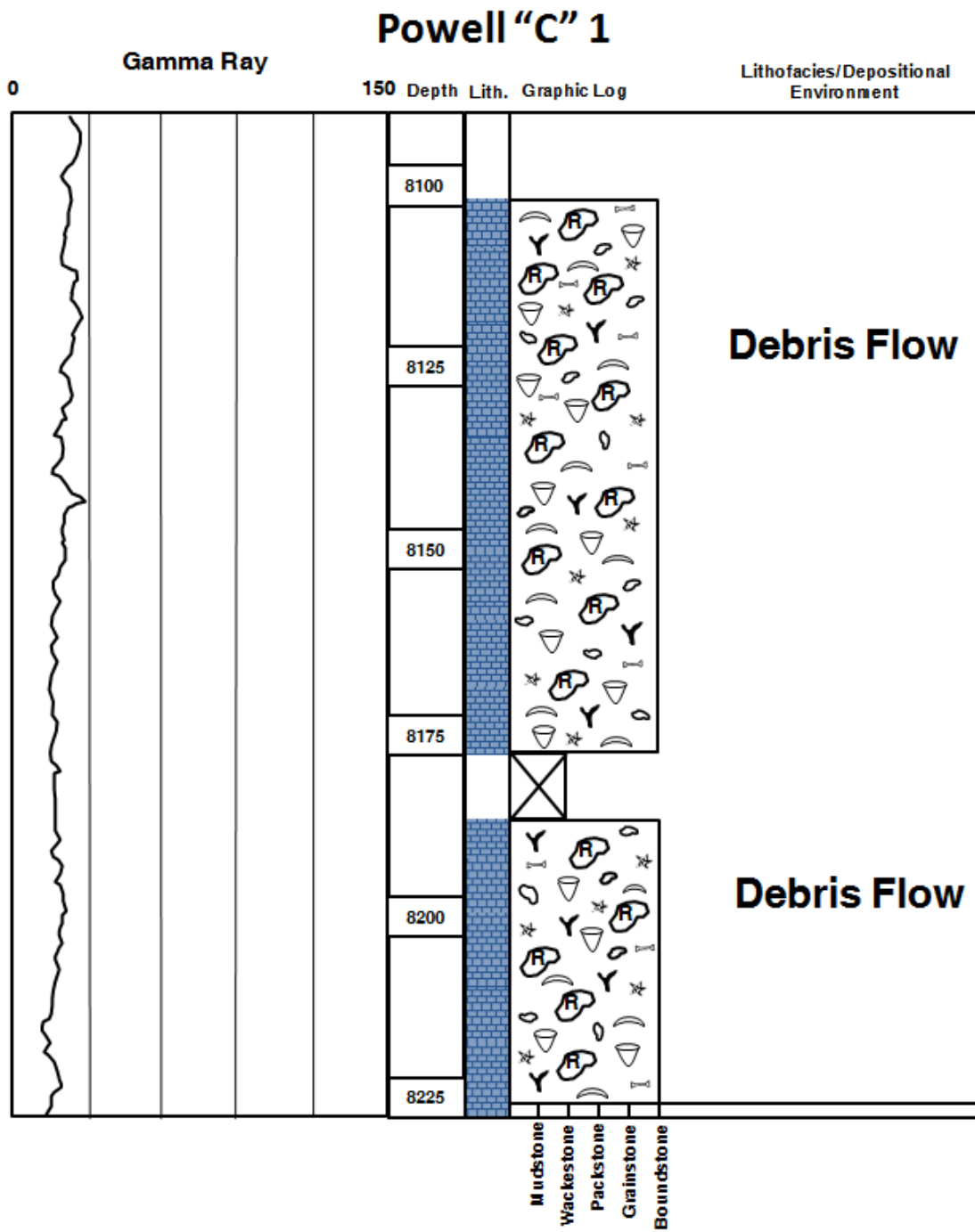


Figure 7: Core description showing *detrital apron debris flow* facies observed in Powell "C" 1 well.

# J. W. Cox #1

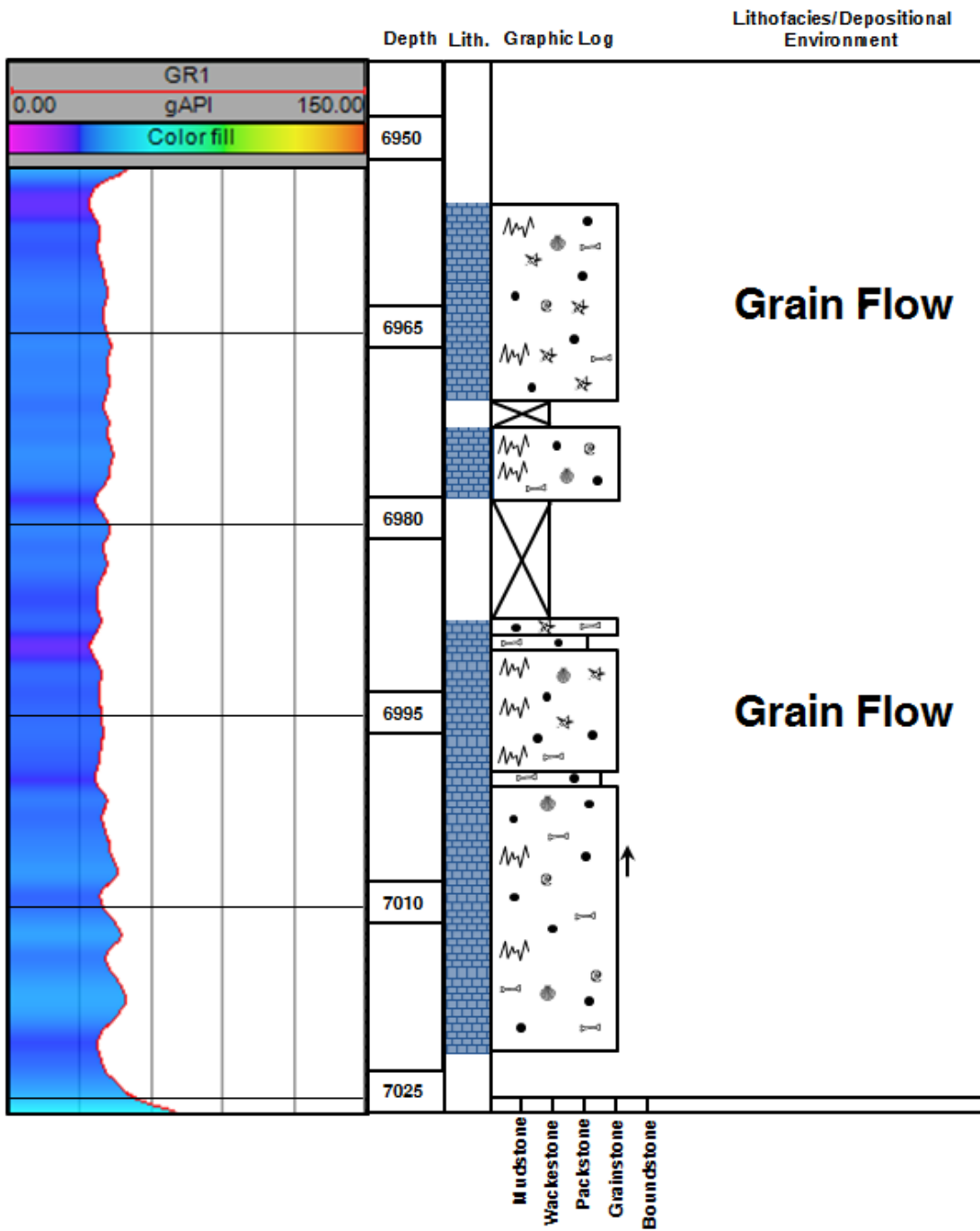


Figure 8: Core description showing *detrital apron grain flow* facies observed in J. W. Cox #1 well.

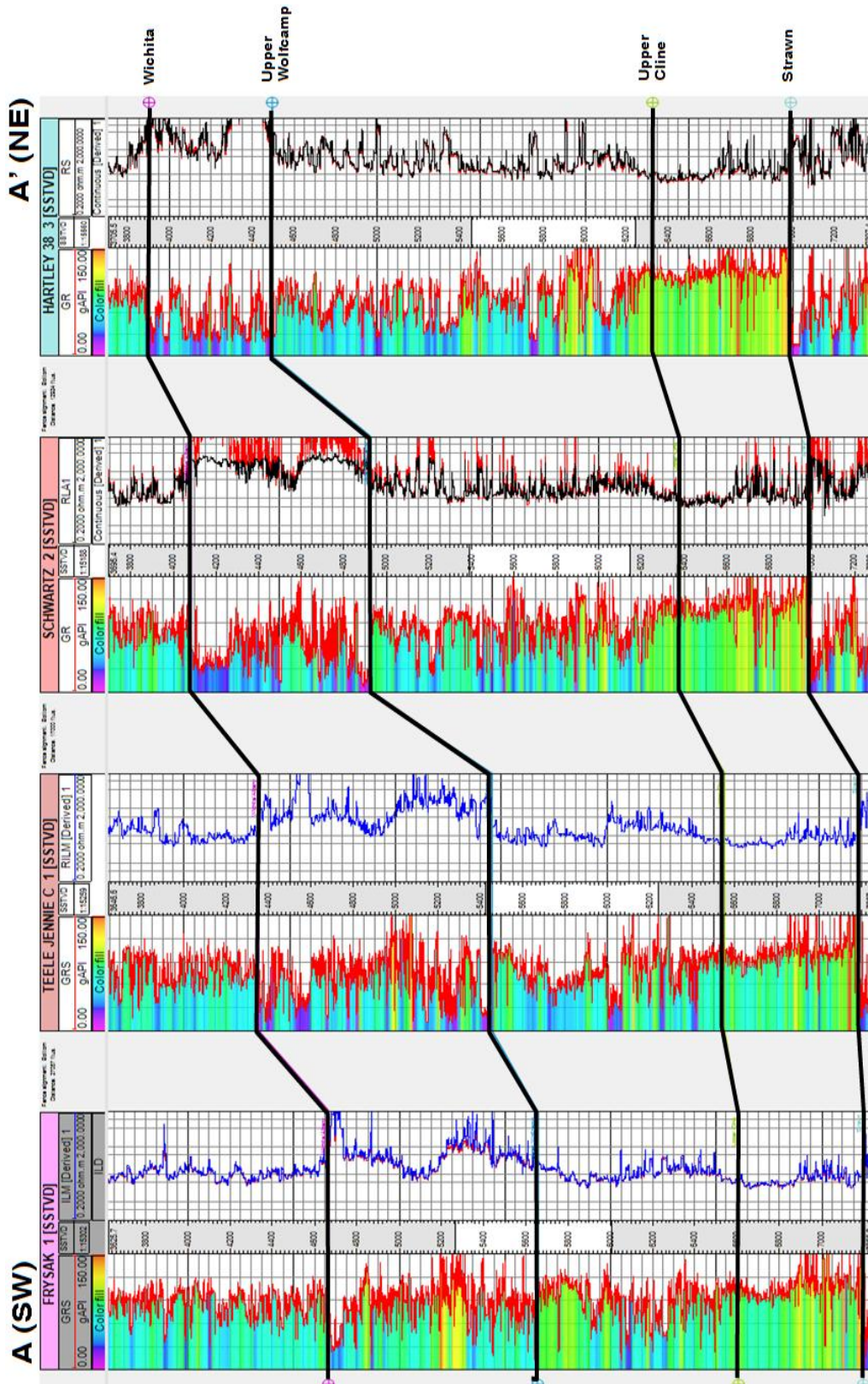


Figure 9: Dip cross section A-A' illustrating gross structure of the Upper Pennsylvanian-Lower Permian strata within the study area.

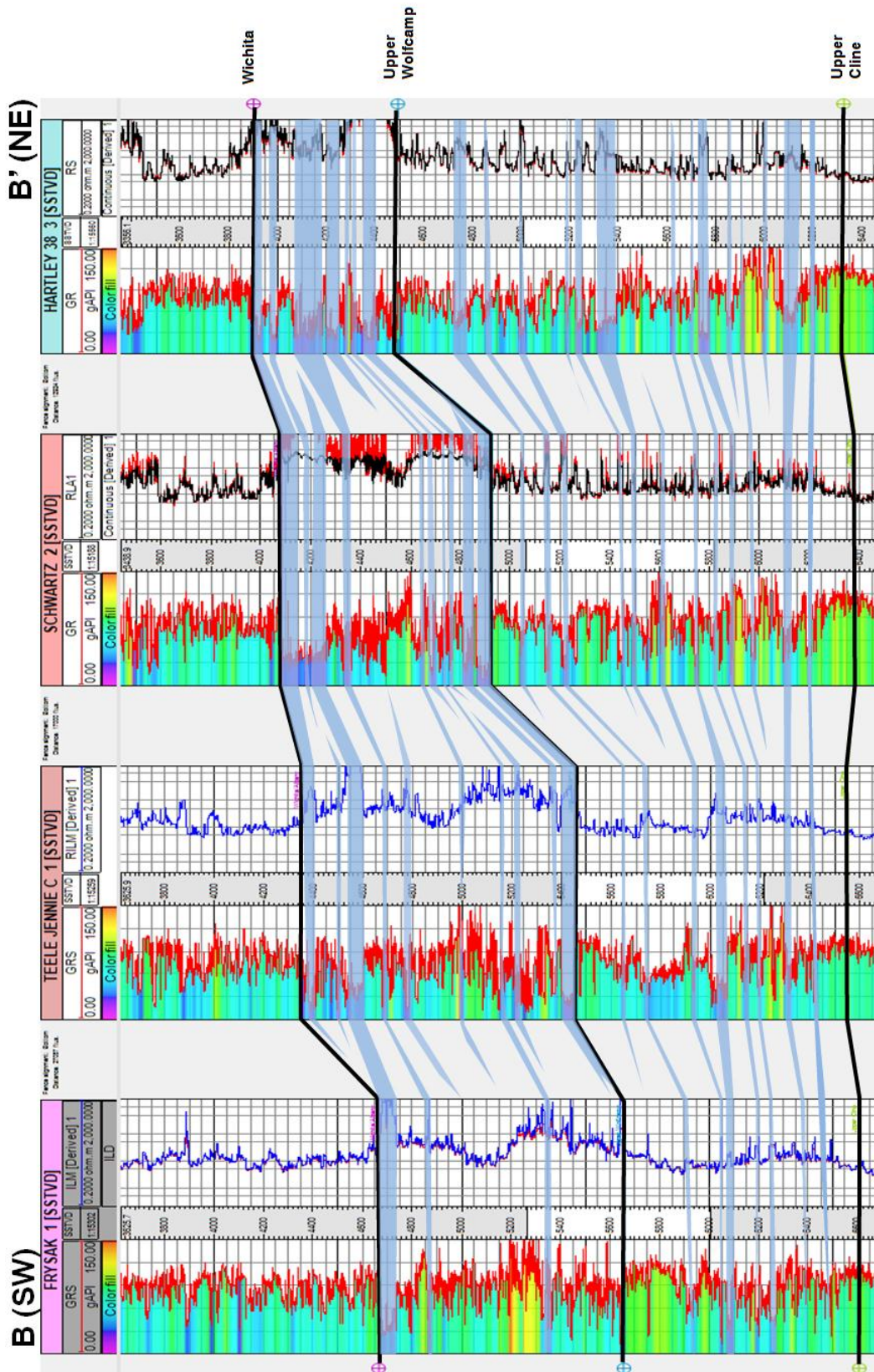


Figure 10: Dip cross section B-B' flattened on the top of Strawn illustrating increase in Wolfcampian-Leonardian paleobathymetric relief and interpretation of detrital carbonate intervals within Wolfcampian-Leonardian strata outlined in blue.

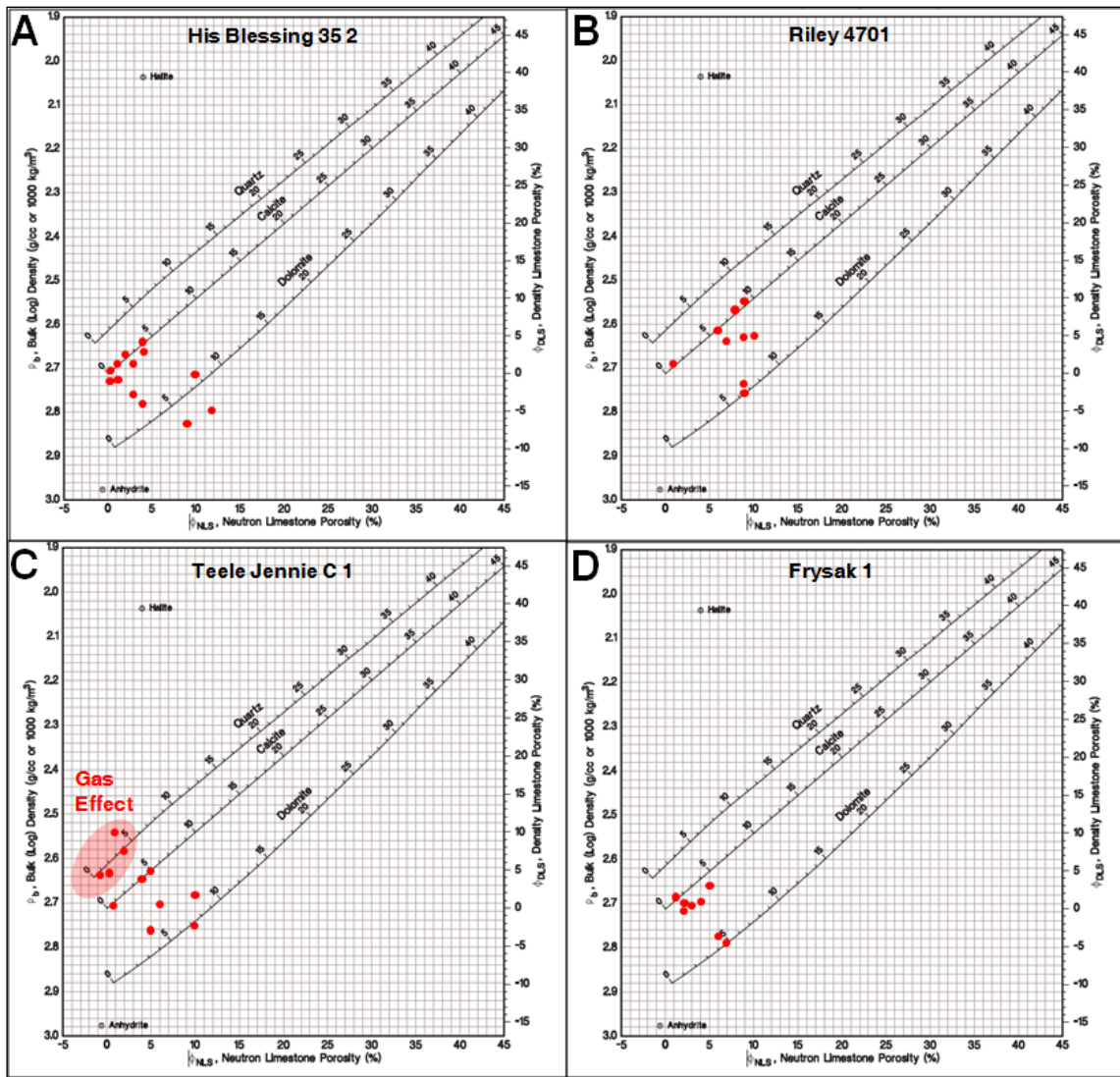
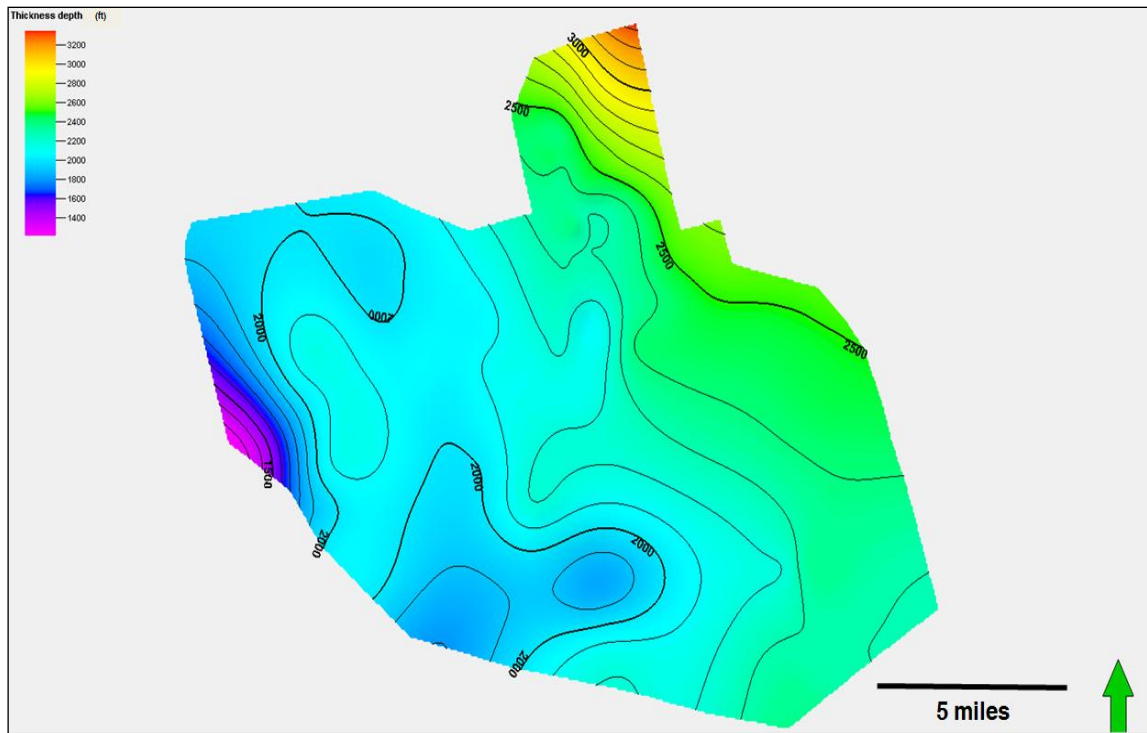


Figure 11: Results from RHOB vs. NPHI crossplot for mineralogical identification of detrital carbonate intervals across a four well dip oriented transect through the study area. A) His Blessing 35-2 is located in closest to the shallow shelf, while D) Fryszak 1 is located the farthest basinward.



**Figure 12: Isochore Map of Wolfcampian-Leonardian section showing substantial basinward thinning.**

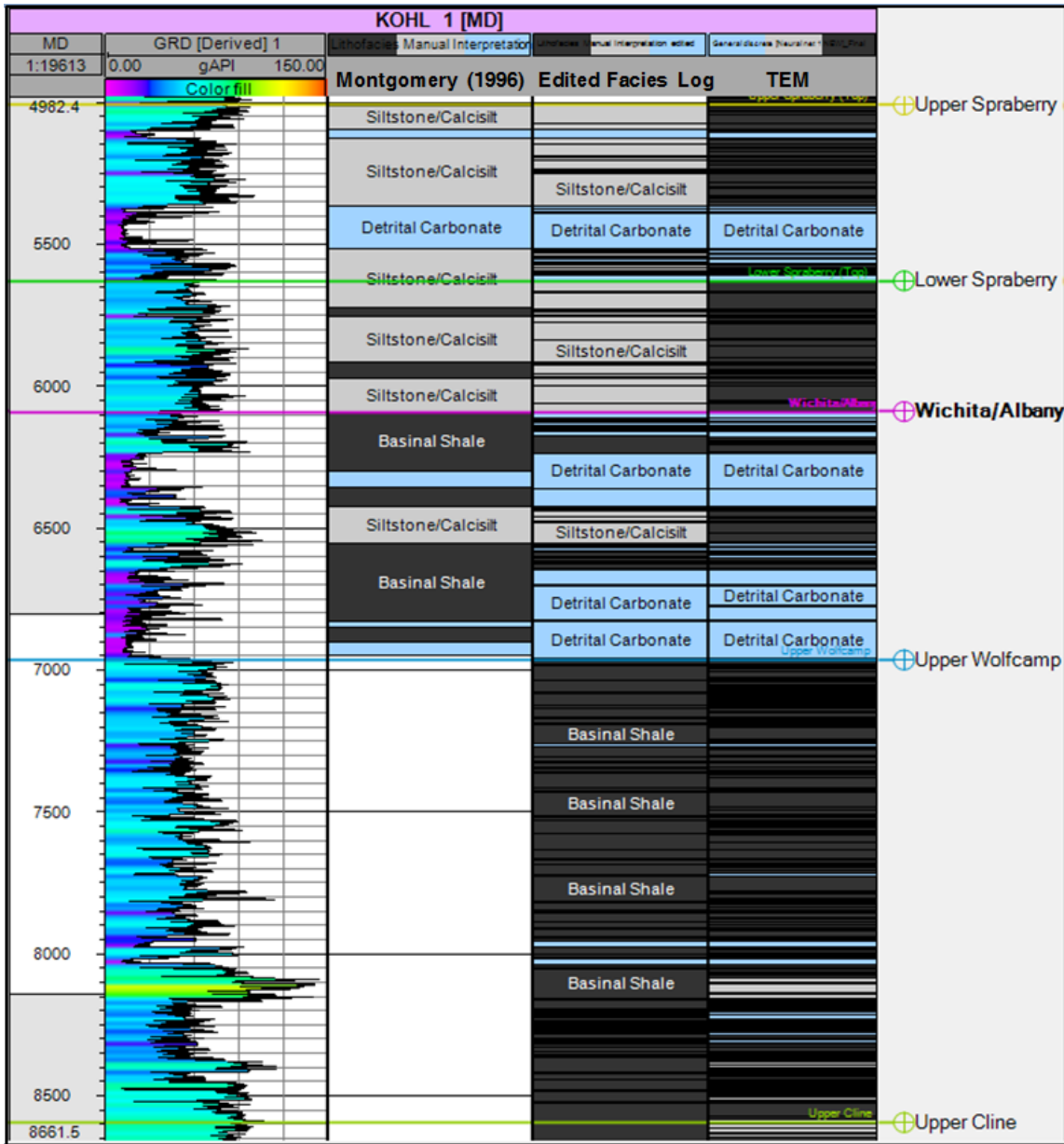


Figure 13: Facies interpretations in Kohl #1 well made by Montgomery (1996), and an edited facies log based on observations from this study which was used to supervise the creation of a facies log using neural networks in the Train Estimation Modeling process in Petrel 2011<sup>®</sup>.



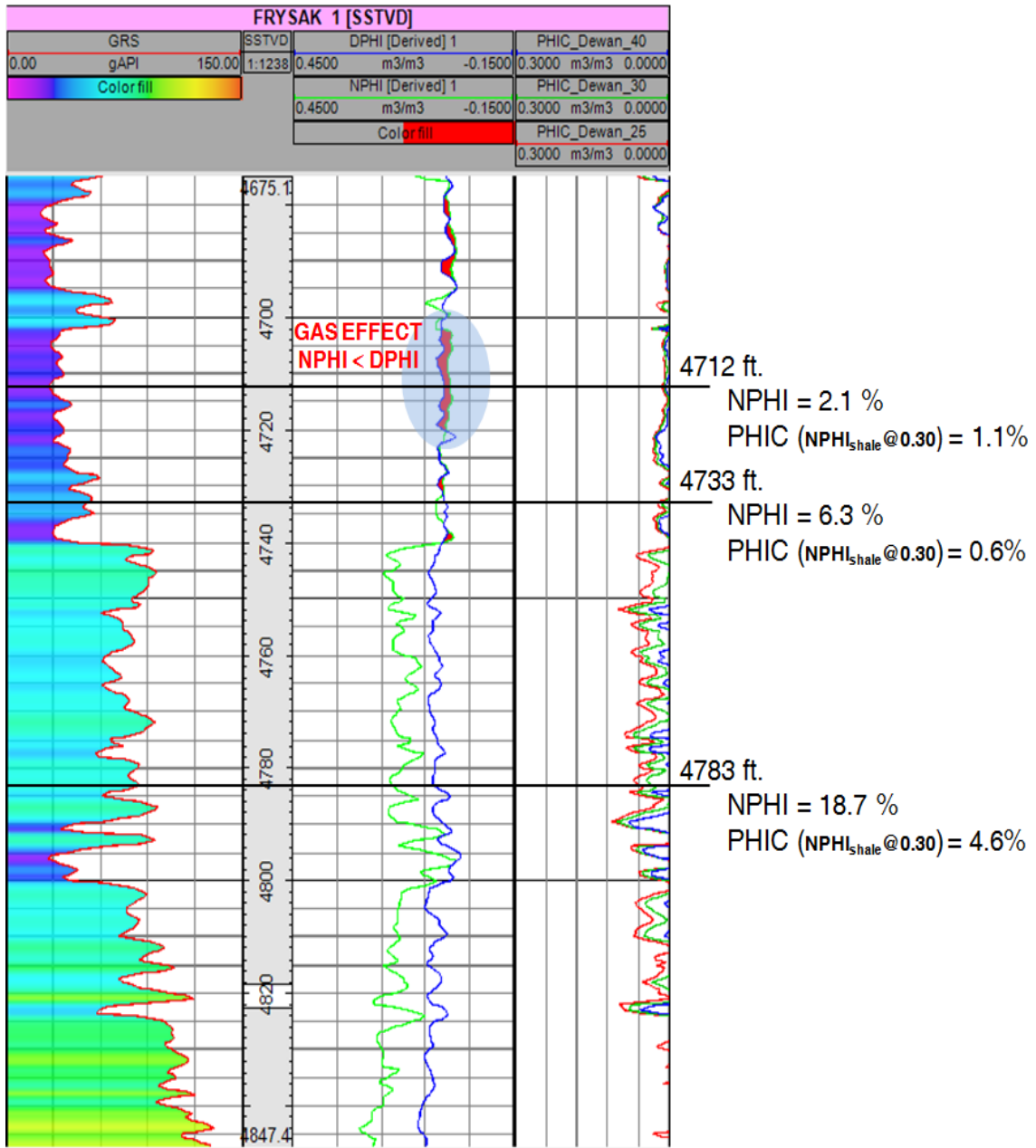


Figure 14: Results of effective porosity estimation from Frysak #1 well.

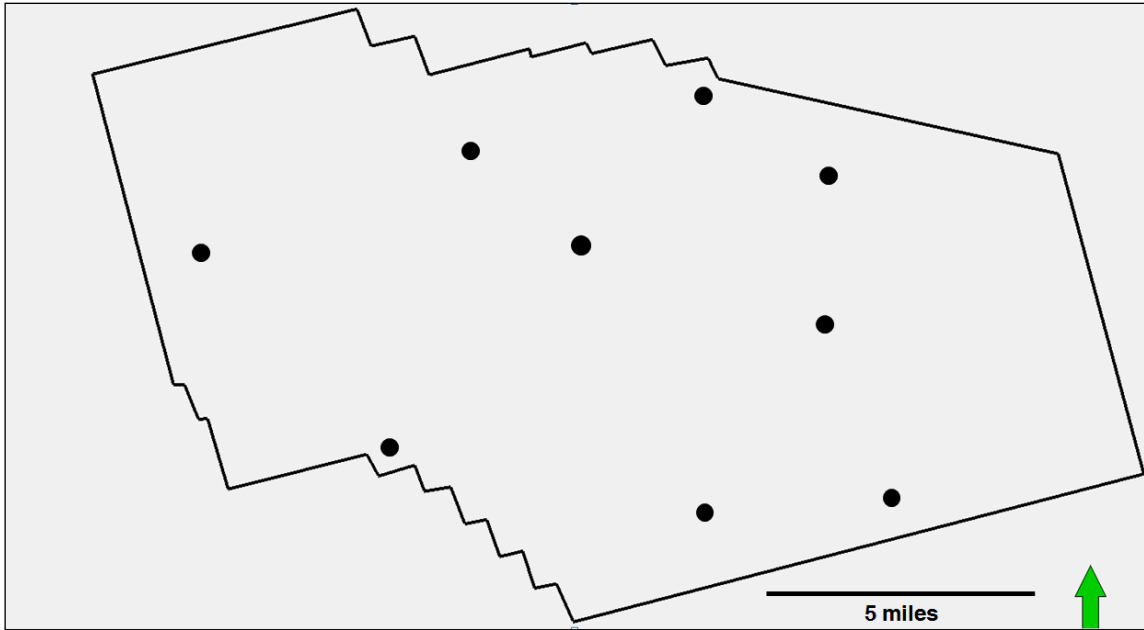


Figure 15: Location of wells used in well-seismic tie process for the 3-D survey.

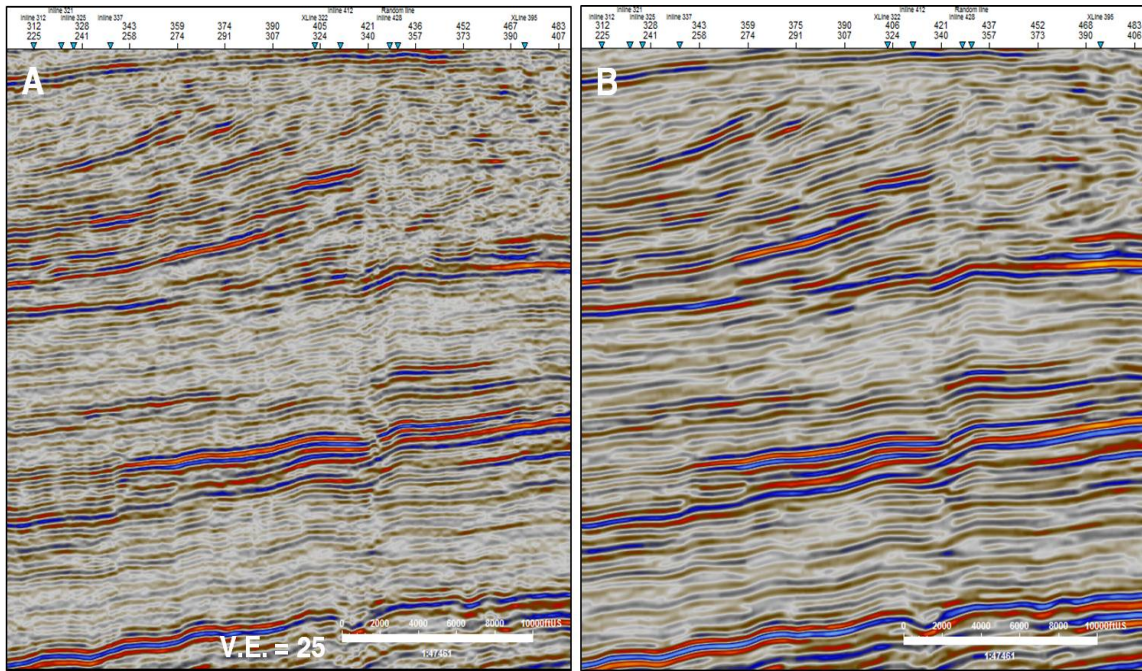


Figure 16: Dip oriented seismic section through 3-D survey comparing the A) original amplitude volume and B) the 3-D volume after undergoing "structural smoothing" process.

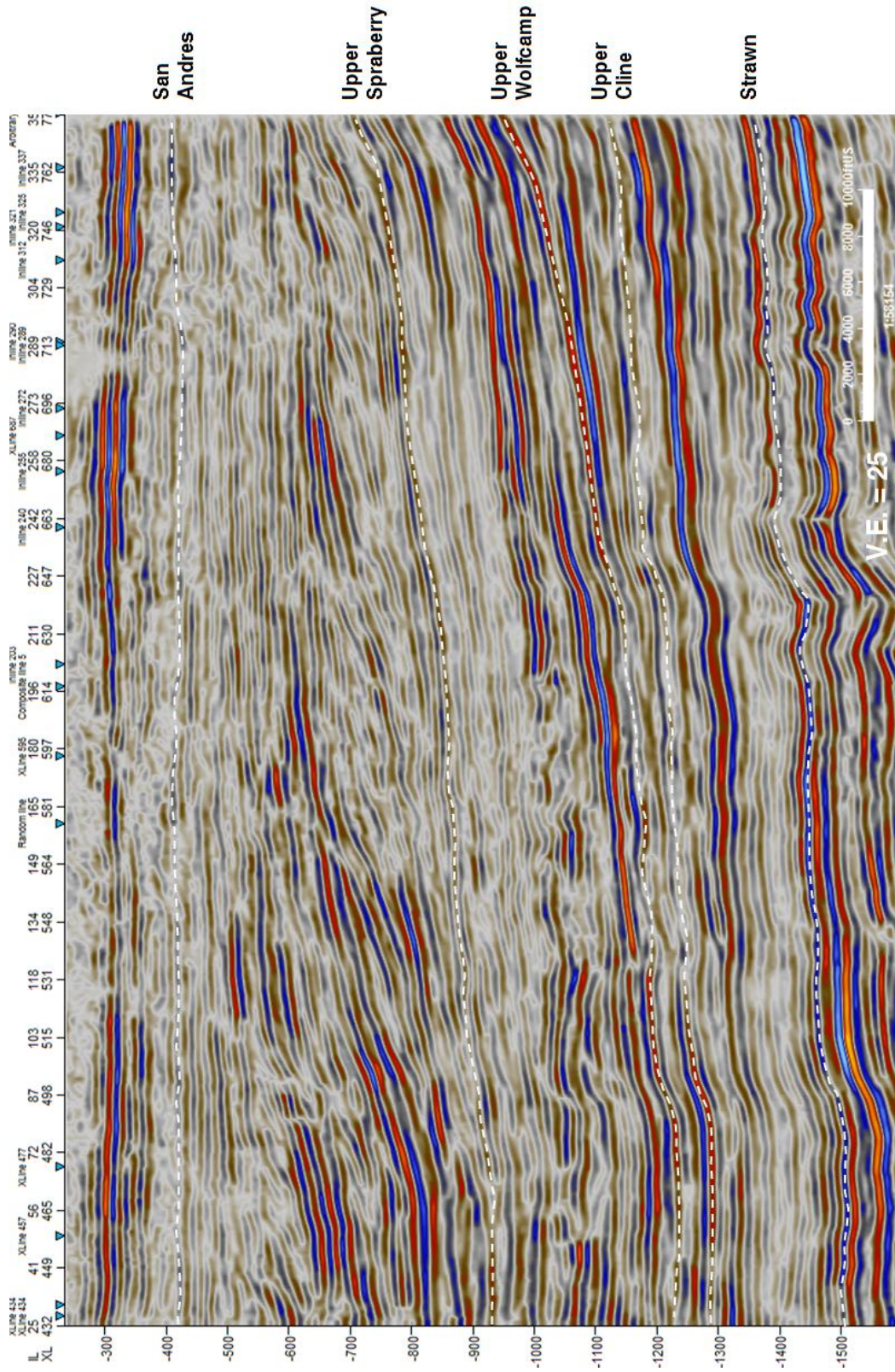
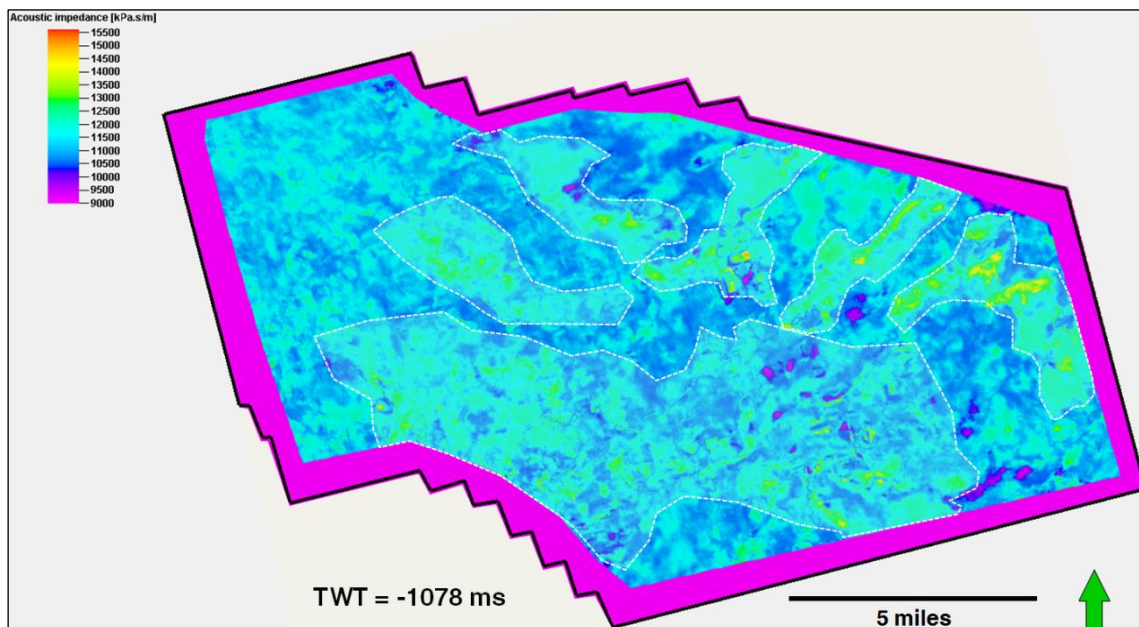
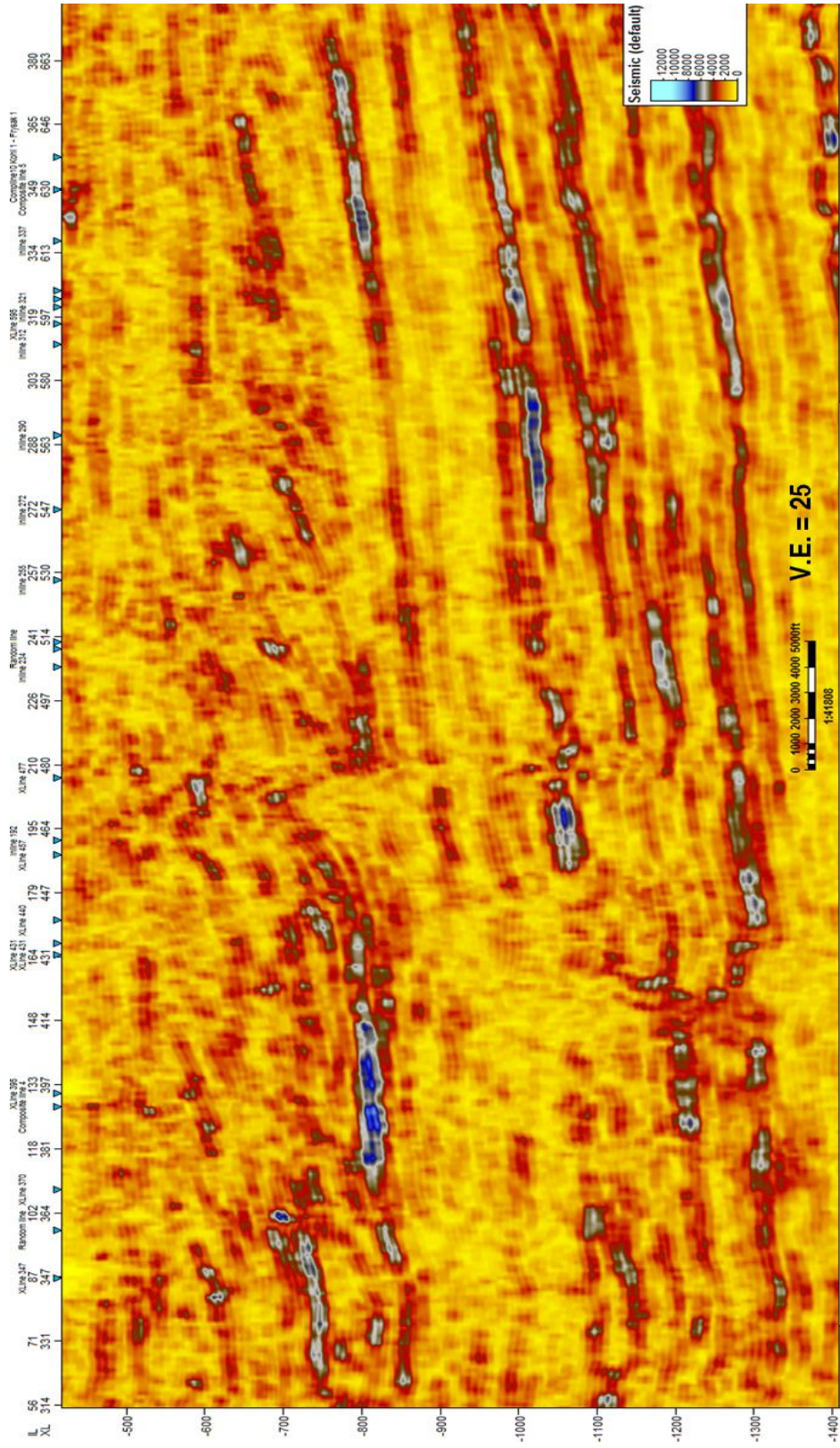


Figure 17: Dip oriented seismic section illustrating gross structure of the Upper Pennsylvanian-Permian strata within the study area. Interpreted horizons shown in dashed white lines.



**Figure 18: Time slice 1078 ms flattened on Upper Wolfcamp horizon through Lower Leonardian section illustrating NE-SW trending acoustic impedance values interpreted as detrital carbonate depositional patterns outlined in white dashed lines.**



**Figure 19: Dip oriented seismic section through RMS amplitude attribute volume. Areas of high RMS amplitude between 700 ms and 1150 ms are interpreted as potential areas of thick detrital carbonate accumulation.**

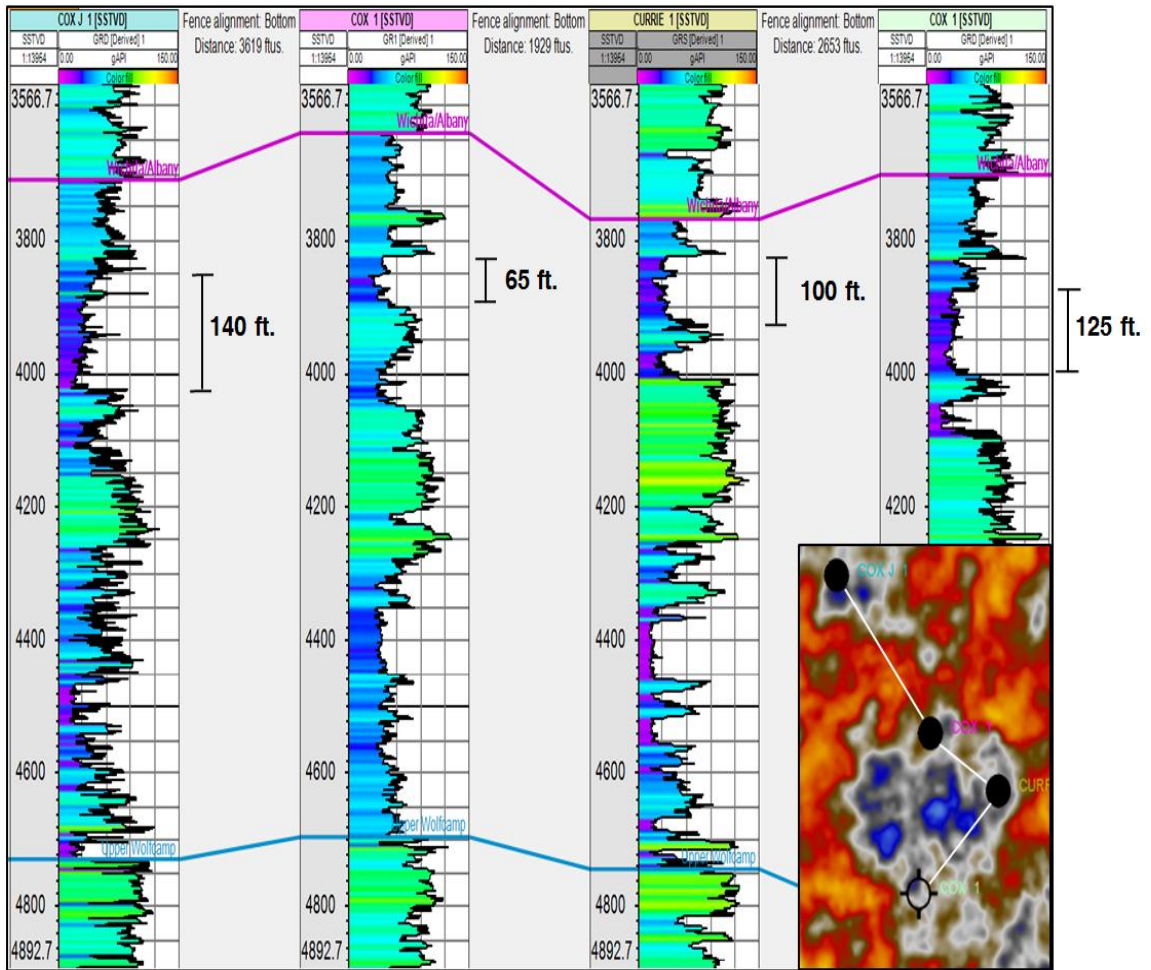


**Figure 20: Cross section through four wells showing detrital carbonate thickness in upper part of Leonardian section and associated RMS amplitude response.**

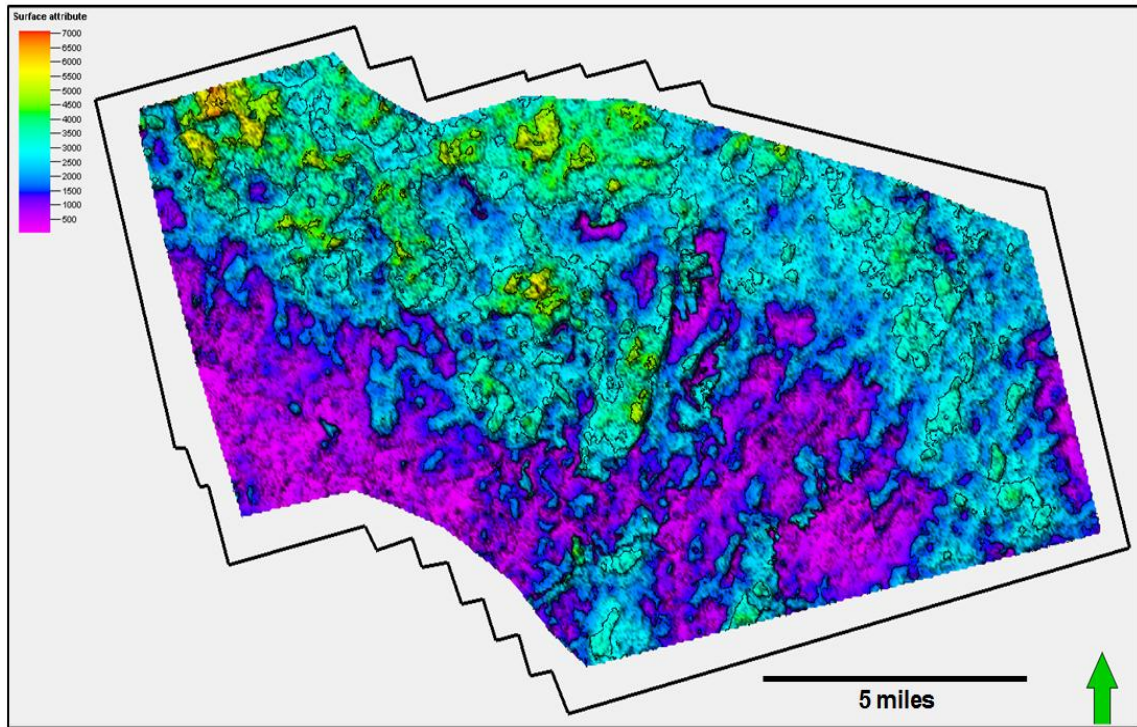


**Figure 21: RMS amplitude extraction along the interpreted Upper Wolfcamp horizon within the study area showing southwest trending high RMS values, interpreted as detrital carbonate accumulation. A large RMS trending northwest towards historically prolific Wolfcampian-Leonardian production in Powell Ranch area.**

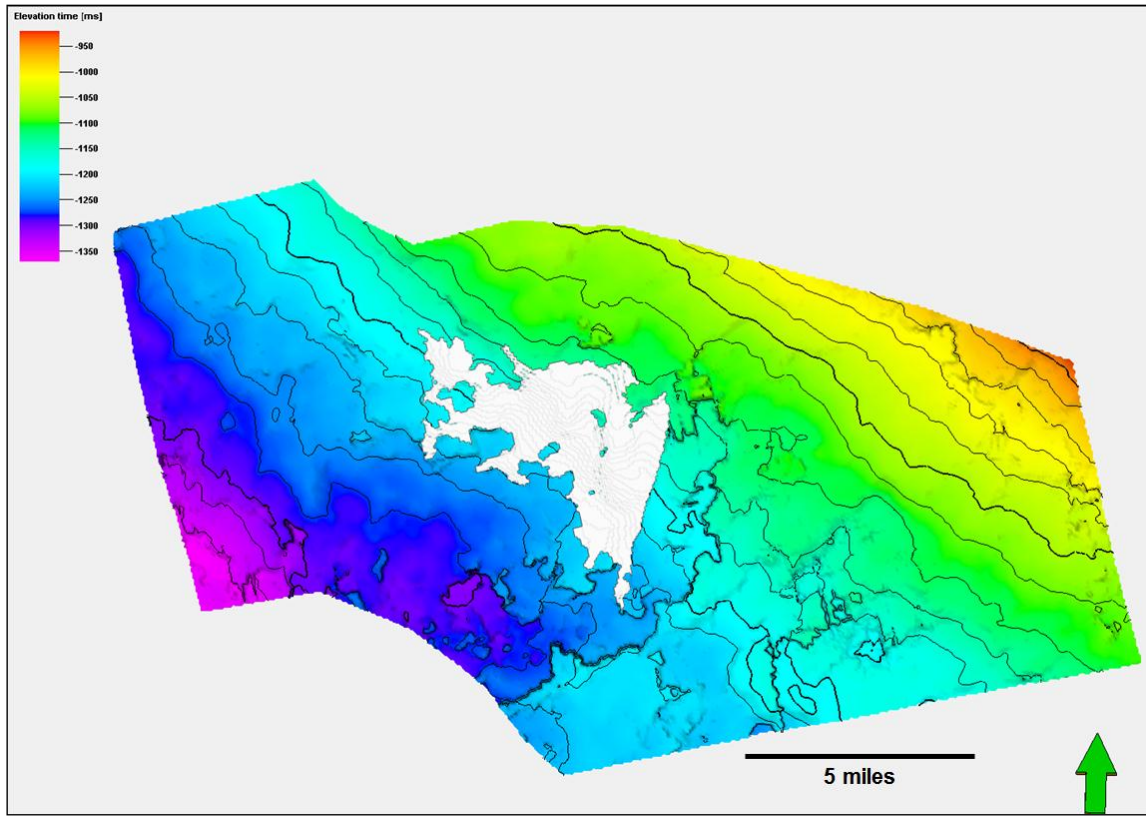


**Figure 22: Seismic geobody (white) extracted from RMS amplitude volume along the Upper Wolfcamp interpreted time horizon (background).**



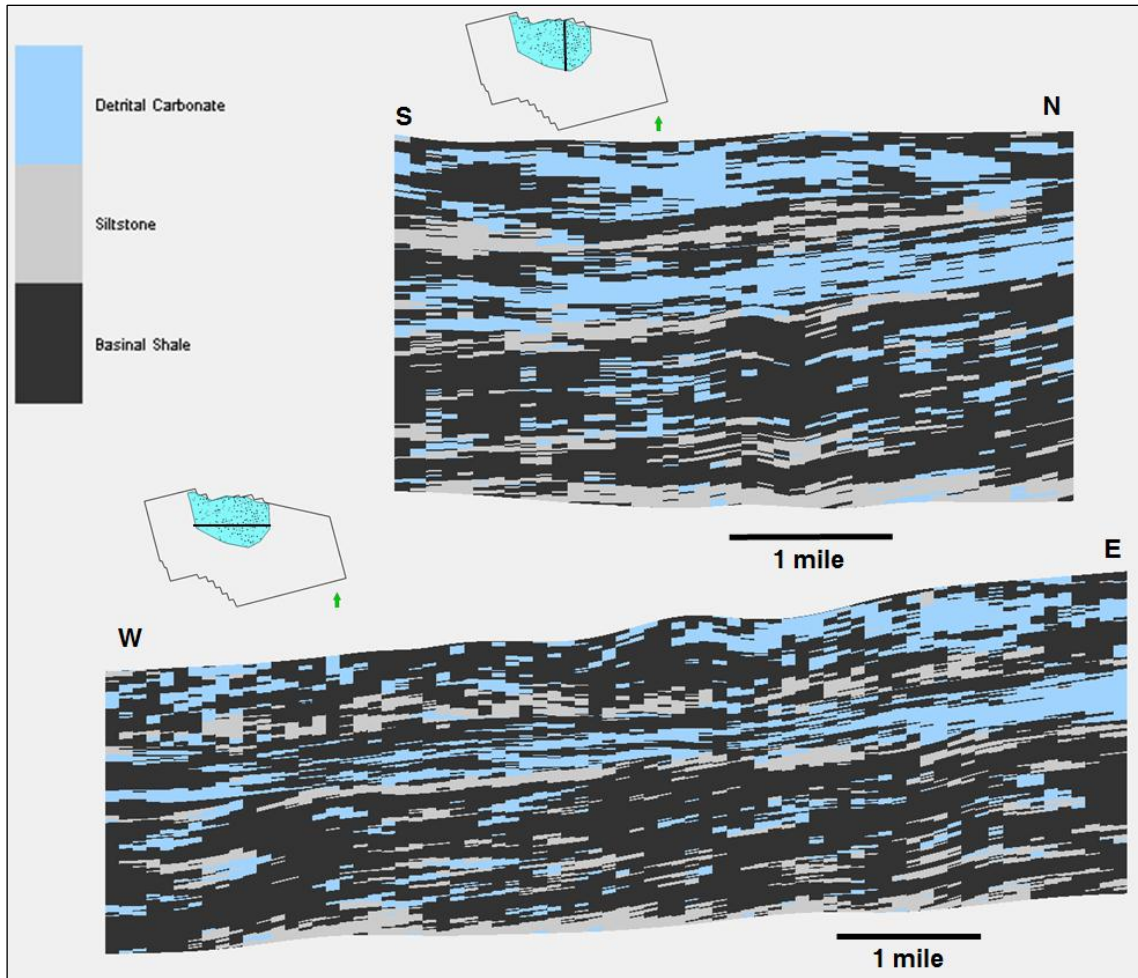
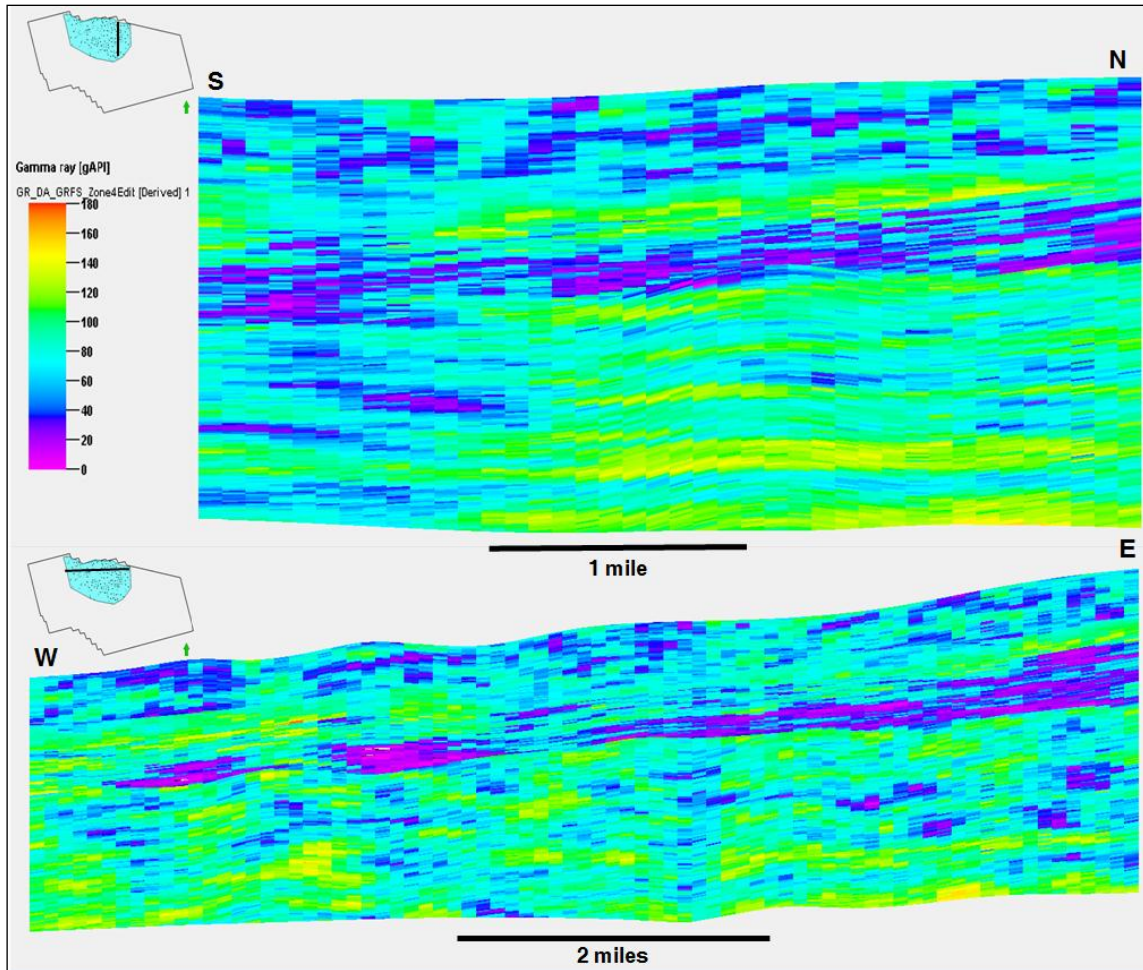
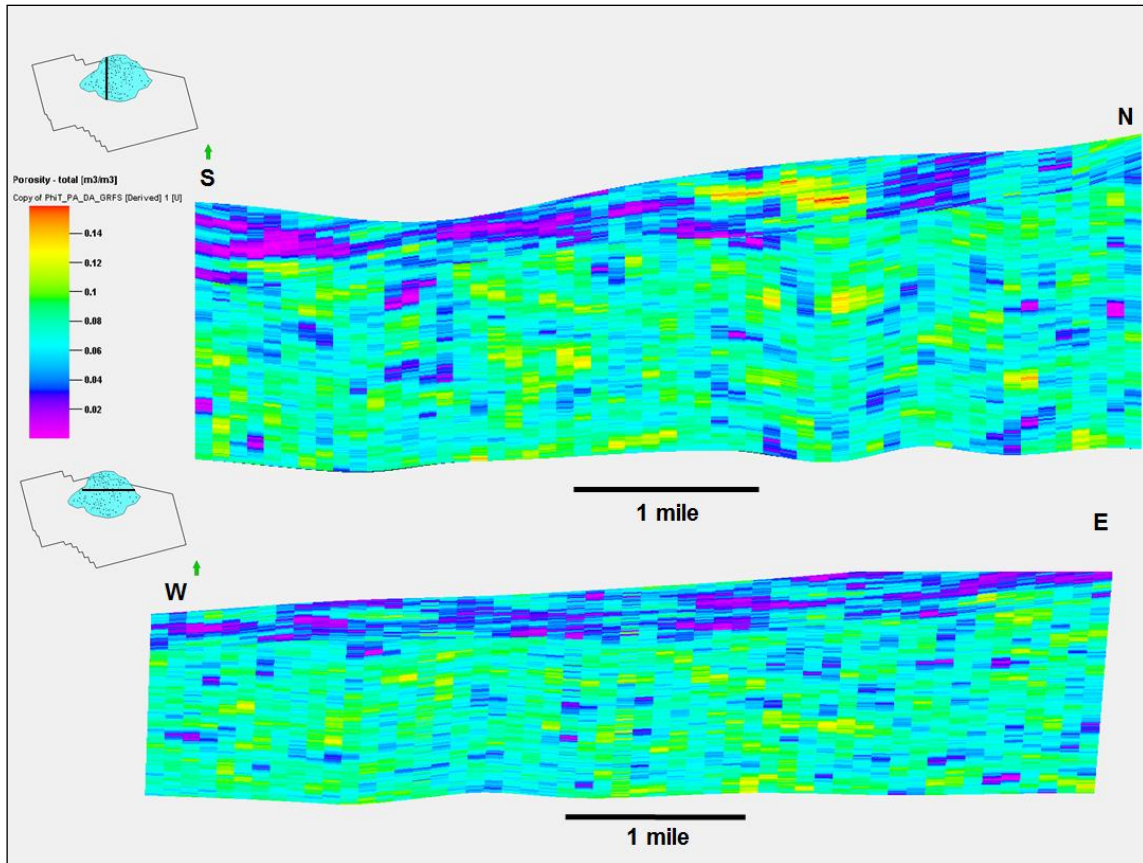


Figure 23: N-S and E-W transects through the lithofacies log property model within the study area. The upper two zones of concentrated *detrital carbonate* and *siltstone* are Lower Leonardian, and the lower zone of mostly *basinal shale* facies is Wolfcampian.



**Figure 24:** N-S and E-W transects through the GR property model within the study area. Low GR values in blue and purple are interpreted as detrital carbonate facies, and higher GR values illustrated in green and yellow are interpreted as basinal shale and siltstone facies.



**Figure 25: N-S and E-W transects through the PHIT property model within the study area. Low PHIT values in blue and purple are interpreted as detrital carbonate facies, and higher PHIT values in green and yellow are interpreted as basinal shale and siltstone facies. A porous detrital carbonate interval with a PHIT exceeding 0.15 is seen in the upper part of the N-S transect (colored yellow/orange/red).**

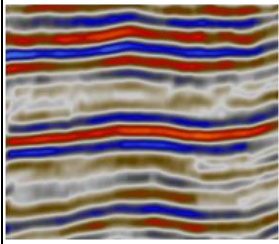
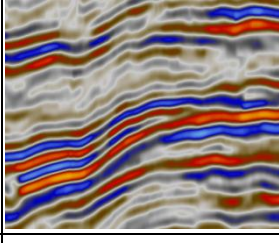
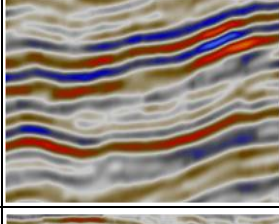
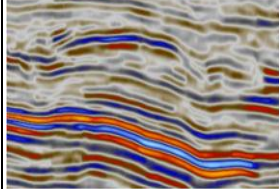
APPENDIX D

TABLES

Facies #	Lithofacies	General Description	Facies Interpretation
1	Clast to matrix-supported wackestone to packstone conglomerate	Light colored skeletal wackestone/packstone to grainstone conglomerate bounded by dark mudstone and calcisilt beds. Coarsens upward from calcisiltstone and matrix supported skeletal wackestone/packstone to a capping clast-supported skeletal grainstone. Brachiopods, bryozoans, fusulinids, and crinoids are observed in the clasts, as well as bivalves in the upper skeletal grainstone cap.	Detrital Apron (Debris Flow)
2	Mudstone with thin brachiopod crinoid fusulinid packstone/grainstone interbeds	Primarily dark grey to black finely laminated mudstone. Several fining upward skeletal packstone/grainstone conglomerates occur at 8899-8903', which grades upward to the mudstone facies. A few thin calcisiltstone and fossil-rich beds occur, but are rare. Carbonate and pyrite nodules observed in mudstone.	Basinal, Deep Water
3	Organic-rich mudstone/wackestone	Dark grey to black color with finely laminated planar beds. Occasional small scale graded beds of calcisiltstone or fine sandstone. Fossils include small brachiopods (1-2 cm), bivalves, crinoid fragments, and fusulinids. Fossil occurrence and density is variable, primarily occurring in concentrated intervals suspended in mudstone matrix. Observed thin beds of wackestone/packstone consisting of randomly oriented brachiopod and crinoid fragments. Pyrite nodules and a single partially filled vertical fracture identified.	Basinal, Deep Water
4	Lithoclast/crinoid-pelletal-skeletal grainstone	Reservoir facies of E.L. Powell #1. Consists entirely of light colored, calcite cemented grainstone and shallow water clasts. Strong hydrocarbon odor/staining with visible interparticle porosity. Dead oil observed within pore space. Fossils within grainstone include brachiopods, crinoids fusulinids, pellets, peloids, and ostracodes. Sharp upper contact formed with an overlying fining-upward lithoclast grainstone. Clasts contain brachiopods, sponges, phylloid algae, and bryozoans. Overlaid by a clast supported crinoid grainstone, but with a dark mudstone matrix.	Detrital Apron (Grain Flow/Distal Turbidite)
5	Clast-supported rudstone with abundant shallow water clasts	Reservoir facies of Powell #1-C. Light colored shallow water clasts with a skeletal packstone/grainstone matrix. Clasts vary in size from 1-2 cm to several 10's of centimeters (estimated from clast size in core), but could be much larger. Clasts are randomly oriented and composed of abundant crinoid, sponge, and phylloid algae fragments. Significant amounts of secondary porosity observed in the form of open vugs throughout the entire section, but no visible porosity identified in the well cemented packstone/grainstone matrix.	Detrital Apron (Debris Flow)

6	Organic-rich dark grey to black shale	Dark grey to black color with fine laminations. Identified as shale as the rock does not readily fizz in dilute hydrochloric acid. A thin, discontinuous horizon of brown silty intraclasts identified at 8162'. A separate interval containing muddy wackestone clasts with abundant crinoid fragments observed near the top of the section, possibly slope derived.	Basinal Deep Water
7	Clast-supported conglomerate with shallow shelf derived clasts	Consists of light colored skeletal packstone/grainstone and rudstone clasts with a dark brown to black mudstone matrix. Clasts consist of abundant shallow water fossils including sponges, bryozoans, large crinoids, and phylloid algae with cement filled fenestrae and voids. Several upright and overturned geopetal structures are observed within clasts at 8104'. Clasts are poorly sorted and show no indication of grading or other sedimentary structures.	Detrital Apron (Debris Flow)
8	Pelletal-skeletal packstone/grainstone	Reservoir facies of J.W. Cox #1. Consists entirely of light tan to light gray pelletal-skeletal packstone/grainstone. Grain size varies from fine to coarse grained pellets and crinoid skeletal fragments. Moderate to well sorted with some larger grainstone fragments occurring locally. Intraparticle porosity is abundant, and stylolitic contacts are observed throughout the core. Massively bedded, with a single graded bed present at 6996'. Mud intraclasts observed near the top of the cored section are 1-3 cm in diameter.	Detrital Apron (Grain Flow/Distal Turbidite)

**Table 1: List of individual facies (1-8) described in four cores used for study.**

Seismic facies	Reflection Configuration	Reflection Continuity	Reflection amplitude and frequency	Bounding relationship	Example
1	Parallel to Semiparallel	Continuous	High Amplitude	Continuous	
2	Semiparallel	Semicontinuous	High Amplitude	Discontinuous and downlapping	
3	Parallel to Semiparallel	Semicontinuous	High and Low amplitude; reflection broadening	Continuous	
4	Mounding	Discontinuous	Internally lower amplitude, externally higher amplitude	Onlap onto mounds; downlap onto lower surfaces; truncation of reflectors	

**Table 2: List of described seismic facies (1-4) and associated characteristics observed in the 3-D volume over the study area. Interpretations were made using the structurally smoothed amplitude volume.**